

# Conversion of Random X-inactivation to Imprinted X-inactivation by Maternal PRC2

Clair Harris<sup>1\*</sup>, Marissa Cloutier<sup>1\*</sup>, Megan Trotter<sup>1</sup>, Michael Hinten<sup>1,2</sup>, Srimonta Gayen<sup>1,3</sup>,  
Zhenhai Du<sup>4</sup>, Wei Xie<sup>4</sup>, and Sundeep Kalantry<sup>1,5</sup>

\*Equal contribution

<sup>1</sup> *Department of Human Genetics, University of Michigan, Ann Arbor, MI, USA*

<sup>2</sup> Current address: Division of Nephrology and Hypertension, Mayo Clinic College of Medicine, Rochester, MN USA

<sup>3</sup> Current address: Department of Molecular Reproduction, Development and Genetics, Indian Institute of Science, Bangalore-560012, India

<sup>4</sup> Center for Stem Cell Biology and Regenerative Medicine, MOE Key Laboratory of Bioinformatics, THU-PKU Center for Life Sciences, School of Life Sciences, Tsinghua University, Beijing, China

<sup>5</sup> Corresponding author ([kalantry@umich.edu](mailto:kalantry@umich.edu))

Keywords: X-chromosome inactivation, imprinting, Polycomb repressive complex 2, epigenetic regulation

## **Abstract**

Imprinted X-inactivation silences genes exclusively on the paternally-inherited X-chromosome and is a paradigm of transgenerational epigenetic inheritance in mammals. Here, we test the role of maternal vs. zygotic Polycomb repressive complex 2 (PRC2) protein EED in orchestrating imprinted X-inactivation in mouse embryos. In maternal-null ( $Eed^{m/-}$ ) but not zygotic-null ( $Eed^{z/-}$ ) early embryos, the maternal X-chromosome ectopically induced *Xist* and underwent inactivation.  $Eed^{m/-}$  females subsequently stochastically silenced *Xist* from one of the two X-chromosomes and displayed random X-inactivation. This effect was exacerbated in embryos lacking both maternal and zygotic EED ( $Eed^{mz/-}$ ), suggesting that zygotic EED can also contribute to the onset of imprinted X-inactivation. *Xist* expression dynamics in  $Eed^{m/-}$  embryos resemble that of early human embryos, which lack oocyte-derived maternal PRC2 and only undergo random X-inactivation. Thus, expression of PRC2 in the oocyte and transmission of the gene products to the embryo may dictate the occurrence of imprinted X-inactivation in mammals.



## **Introduction**

X-chromosome inactivation results in the mitotically-stable transcriptional inactivation of one of the two X-chromosomes in female mammals in order to equalize X-linked gene expression between males and females (Morey & Avner, 2011; Plath, Mlynarczyk-Evans, Nusinow, & Panning, 2002). Two different forms of X-inactivation characterize the mouse embryo, imprinted and random. Imprinted X-inactivation results in the exclusive silencing of genes on the paternal X-chromosome and initiates during preimplantation embryogenesis (Huynh & Lee, 2003; Mak et al., 2004; Monk & Kathuria, 1977; Okamoto, Otte, Allis, Reinberg, & Heard, 2004; Takagi & Sasaki, 1975). In the post-implantation embryo, imprinted X-inactivation is stably maintained in the extraembryonic lineage but reversed in the embryonic lineage (Harper, Fosten, & Monk, 1982; Mak et al., 2004; Okamoto et al., 2004; Takagi & Sasaki, 1975; West, Frels, Chapman, & Papaioannou, 1977), which subsequently undergoes random inactivation of either the maternal or the paternal X-chromosome (Lyon, 1961). Notably, imprinted X-inactivation is a paradigm for both mitotic as well as meiotic, or transgenerational, epigenetic regulation, due to its stable parent-of-origin-specific inactivation pattern.

X-inactivation is characterized by a well-defined series of epigenetic events (Kalantry, 2011). Both imprinted and random X-inactivation are prefaced by the expression of X-linked non-protein coding Xist RNA from the prospective inactive-X (Kay, Barton, Surani, & Rastan, 1994; Penny, Kay, Sheardown, Rastan, & Brockdorff, 1996). During imprinted X-inactivation in the mouse embryo, *Xist* is expressed at the two-cell stage and the RNA visibly begins to coat the paternal-X at the four-cell stage (Kalantry, Purushothaman, Bowen, Starmer, & Magnuson, 2009; Namekawa, Payer, Huynh, Jaenisch, & Lee, 2010; Patrat et al., 2009). The progressive accumulation of Xist RNA coincides with the gradual and stereotyped silencing of paternal X-linked genes that is only completed after the blastocyst stage of embryogenesis (Kalantry et al., 2009; Namekawa et al., 2010; Patrat et al., 2009). Coincident with Xist RNA coating, PRC2

proteins and H3K27me3 accumulate on the inactive-X, correlating with the silencing of X-linked genes (Mak et al., 2004; Okamoto et al., 2004; Plath et al., 2003; Silva et al., 2003). Moreover, the mis-expression of *Xist* results in the concomitant accumulation of PRC2 proteins and H3K27me3 (de la Cruz et al., 2005; Kohlmaier et al., 2004; Plath et al., 2003; Silva et al., 2003), suggesting that *Xist* RNA directly or indirectly recruits PRC2 to the inactive-X. PRC2 has thus been suggested to contribute to the establishment of X-inactivation (Plath et al., 2003; Silva et al., 2003).

Consistent with a role for PRC2 in X-inactivation, we and others previously showed that post-implantation female mouse embryos mutant for the Polycomb gene *Eed* fail to maintain silencing of paternal X-linked genes during imprinted X-inactivation (Kalantry & Magnuson, 2006; Kalantry et al., 2006; J. Wang et al., 2001). EED is a non-catalytic component of the PRC2 complex, but EED binding to the PRC2 enzyme EZH2 is required for the methyltransferase activity of EZH2 (Cao et al., 2002; Czermin et al., 2002; Kuzmichev, Nishioka, Erdjument-Bromage, Tempst, & Reinberg, 2002; Muller et al., 2002). When EED is mutated other core PRC2 proteins are degraded and H3K27me3 is lost (Montgomery et al., 2005). Thus, EED is an essential component of PRC2 and EED function is canonically equated with H3K27me3 catalysis (Margueron & Reinberg, 2010; Montgomery et al., 2005).

Although *Eed*<sup>-/-</sup> embryos fail to maintain imprinted X-inactivation, they initiate imprinted X-inactivation properly (Kalantry & Magnuson, 2006; Kalantry et al., 2006). A potential answer for this difference is that *Eed*<sup>-/-</sup> embryos inherit maternal EED protein that is present in the oocyte (Kalantry & Magnuson, 2006; Plath et al., 2003; Shumacher, Faust, & Magnuson, 1996). The presence of maternally-derived EED protein could explain the absence of a defect in establishing imprinted X-inactivation in *Eed*<sup>-/-</sup> embryos. Such maternal control of imprinted X-inactivation would also be consistent with a transgenerational epigenetic effect that underlies genomic imprinting (Barlow, 2011; Ferguson-Smith & Bourc'his, 2018; Lee & Bartolomei, 2013;

van Otterdijk & Michels, 2016). Here, we test the hypothesis that oocyte-derived PRC2 orchestrates imprinted X-inactivation in the early embryo.

## **Results**

### **EED and H3K27me3 Enrichment on the Inactive-X in *Eed*<sup>-/-</sup> Embryos**

PRC2 proteins and H3K27me3 are first enriched on the prospective inactive X-chromosome in the early mouse embryo at the 8-16 cell morula stage (Okamoto et al., 2004). We assessed the accumulation of EED and H3K27me3, and Xist RNA by immunofluorescence (IF) combined with fluorescent *in situ* hybridization (FISH) in wild-type (WT) embryonic day (E) 3.5 blastocyst embryos (Cloutier, Harris, Gayen, Maclary, & Kalantry, 2018; Hinten, Maclary, Gayen, Harris, & Kalantry, 2016), which are in the process of silencing X-linked genes and establishing imprinted X-inactivation (Borensztein et al., 2017; Namekawa et al., 2010; Patrat et al., 2009; F. Wang et al., 2016). As expected, females displayed coincident accumulation of EED, H3K27me3, and Xist RNA in a vast majority of the nuclei (72-100%). Males, by contrast, lacked such enrichment (Figure 1A).

Our previous work suggested that zygotically-null preimplantation embryos harbor WT maternal EED protein (Kalantry & Magnuson, 2006; Kalantry et al., 2006). To test for the presence of maternally-derived EED protein in *Eed*<sup>-/-</sup> embryos, we employed our previously generated conditional *Eed* mutation (Figure 1- figure supplement 1A) (Maclary et al., 2017). We generated E3.0-E3.5 blastocyst-stage embryos zygotically-null and heterozygous for *Eed* (*Eed*<sup>-/-</sup> and *Eed*<sup>+/-</sup>, respectively) from a cross of *Eed*<sup>+/-</sup> females with *Eed*<sup>fl/-</sup>; *Prm-Cre* males. *Prm-Cre* is active during spermatogenesis and catalyzes the deletion of the *loxP* flanked (floxed) *Eed* allele in the mature sperm (Figure 1- figure supplement 1B) (O'Gorman, Dagenais, Qian, & Marchuk, 1997). As a result, half of the embryos generated from the above cross are expected to be genotypically *Eed*<sup>-/-</sup> and the other half *Eed*<sup>+/-</sup>. In the derived embryos, we assayed inactive-X enrichment of EED, H3K27me3, and Xist RNA by combined IF/FISH (Figure 1B). Of the 41

female embryos examined, nine showed coincident accumulation of EED and/or H3K27me3 with Xist RNA in over 70% of the nuclei and are not significantly different from WT embryos in Figure 1A ( $p>0.1$ ). An additional nine embryos were devoid of EED or H3K27me3 enrichment overlapping with the Xist RNA coat. We presumed the former to be *Eed*<sup>+/-</sup> embryos and the latter to be *Eed*<sup>-/-</sup> embryos. An additional 23 embryos displayed 2-70% of nuclei with EED and/or H3K27me3 enrichment. This intermediate class likely represents *Eed*<sup>+/-</sup> or *Eed*<sup>-/-</sup> embryos that have not yet fully depleted maternally-inherited EED protein or *Eed*<sup>+/-</sup> embryos that have not yet robustly expressed zygotic EED. Male embryos from the cross, distinguished by a lack of Xist RNA coating, did not show enrichment of EED or H3K27me3 in the nucleus, as in the WT male embryos in Figure 1A.

To confirm that there is no bias in the sex ratio or genotype of the embryos, we performed PCR genotyping of embryos derived from the above cross (Figure 1C). Embryos from 12 litters showed no statistical difference in the distribution of *Eed*<sup>+/-</sup> and *Eed*<sup>-/-</sup> male or female embryos ( $p>0.05$ ), suggesting that the intermediate class of 23 embryos in Figure 1A are likely a mixture of *Eed*<sup>+/-</sup> or *Eed*<sup>-/-</sup> embryos. Together, the results in Figure 1 suggest that genotypically null *Eed*<sup>-/-</sup> embryos inherit oocyte-derived maternal EED protein and that expression of EED transitions from maternal to zygotic at or slightly before the blastocyst stage.

To define the kinetics of depletion of maternal EED and induction of zygotic EED prior to the blastocyst stage, we quantified EED and H3K27me3 IF signals in 2-, 4-, 8-, and 16-cell embryos from the following series of crosses. The first cross was *Eed*<sup>fl/fl</sup> females crossed to *Eed*<sup>fl/fl</sup> males, which yielded control *Eed*<sup>fl/fl</sup> embryos. The second was a cross of *Eed*<sup>fl/-</sup> females to *Eed*<sup>fl/-</sup>; *Prm-Cre* males to generate *Eed*<sup>fl/-</sup> and *Eed*<sup>-/-</sup> embryos (*Eed*<sup>fl/-</sup> / *Eed*<sup>-/-</sup>). Whereas both *Eed*<sup>fl/-</sup> and *Eed*<sup>-/-</sup> embryos are expected to harbor maternal EED protein, *Eed*<sup>fl/-</sup> but not *Eed*<sup>-/-</sup> embryos would express zygotic EED. The third cross was of *Eed*<sup>fl/fl</sup>; *Zp3-Cre* females to WT males to yield embryos which are devoid of maternal EED (*Eed*<sup>m-/-</sup>) but are capable of expressing zygotic EED.

*Zp3-Cre* is active in the growing oocyte, where it efficiently deletes the *Eed<sup>fl</sup>* allele and generates embryos devoid of maternal EED (Figure 5C and Figure 2- figure supplement 1A) (Lewandoski, Wassarman, & Martin, 1997). The final cross was a cross of *Eed<sup>fl/fl</sup>;Zp3-Cre* females with *Eed<sup>fl/fl</sup>;Prm-Cre* males to generate embryos devoid of both maternal and zygotic EED (*Eed<sup>mz/-</sup>*).

*Eed<sup>fl/fl</sup>* and *Eed<sup>fl/-</sup> / Eed<sup>+/-</sup>* 2-cell embryos exhibited similar levels of EED and H3K27me3, whereas *Eed<sup>m/-</sup>* and *Eed<sup>mz/-</sup>* embryos were devoid of both EED and H3K27me3 (Figure 2A, 2C, and 2D; Supplementary File 1). These data are consistent with the 2-cell embryo harboring only maternally-derived EED and H3K27me3. Four-cell embryos displayed a similar pattern to 2-cell embryos, although a subset of *Eed<sup>fl/-</sup> / Eed<sup>+/-</sup>* ~4-cell embryos displayed reduced EED and H3K27me3 levels, consistent with zygotic EED expression beginning at this stage and its failure in *Eed<sup>+/-</sup>* embryos (Figure 2C and Figure 2- figure supplement 1B; Supplementary File 1). At the ~8-cell stage, *Eed<sup>fl/-</sup> / Eed<sup>+/-</sup>* embryos showed highly variable EED and H3K27me3 levels, suggesting further differentiation of the two genotypes. In agreement with increasing zygotic *Eed* expression, *Eed<sup>m/-</sup>* ~8-cell embryos displayed higher levels of EED and H3K27me3 than the corresponding *Eed<sup>mz/-</sup>* embryos (Figure 2C and Figure 2- figure supplement 1B; Supplementary File 1). By the ~16-cell stage, *Eed<sup>fl/-</sup> / Eed<sup>+/-</sup>* embryos are clearly separated into two categories. One group has statistically lower levels of EED, while the other group is statistically indistinguishable from the *Eed<sup>fl/fl</sup>* embryos (Figure 2B, 2C, and 2D; Supplementary File 1). Therefore, the likely genotypes of the two groups are *Eed<sup>+/-</sup>* and *Eed<sup>fl/-</sup>*, respectively. *Eed<sup>m/-</sup>* 16-cell embryos continue to display higher levels of EED and H3K27me3 than the *Eed<sup>mz/-</sup>* embryos, but nevertheless harbor significantly lower EED and H3K27me3 levels than *Eed<sup>fl/fl</sup>* embryos (Figure 2B, 2C, and 2D; Supplementary File 1). In order to visualize how EED levels are changing across early embryogenesis, we plotted the mean values of each genotype by embryonic stage (Figure 2E). Maternally-derived EED starts declining at the 4-cell stage but is

still present at the 16-cell stage. Conversely, while zygotic *Eed* transcription initiates at ~4-cell stage, zygotic EED levels are still low at the ~16-cell stage, suggesting that EED in WT *Eed*<sup>fl/fl</sup> 16-cell embryos is a combination of maternally-derived and zygotically generated protein (Figure 2F).

### **Imprinted X-inactivation Initiation in *Eed*<sup>-/-</sup> Embryos**

To test if zygotic *Eed*<sup>-/-</sup> embryos initiate and establish imprinted X-inactivation, we compared X-linked gene expression in an allele-specific manner in individual hybrid *Eed*<sup>fl/fl</sup>, *Eed*<sup>fl/-</sup>, and *Eed*<sup>-/-</sup> E3.5 blastocysts by RNA sequencing (RNA-Seq) (Figure 3- figure supplement 1A). In these embryos, the maternal X chromosome was derived from the *Mus musculus* 129/S1 mouse strain and the paternal-X from the divergent *Mus molossinus* JF1/Ms strain (Materials and Methods). We exploited single nucleotide polymorphisms (SNPs) to assign RNA-Seq reads to either the maternal or paternal X-chromosome in the hybrid embryos (Cloutier et al., 2018; Maclary et al., 2017). A subset of X-linked genes was expressed more robustly from the paternal allele relative to the maternal allele in *Eed*<sup>fl/-</sup> and *Eed*<sup>-/-</sup> female embryos compared to *Eed*<sup>fl/fl</sup> embryos (Figure 3A; Supplementary File 2). However, when the allelic expression ratio of all X-linked genes in Figure 3A was averaged, paternal X-linked gene expression was not significantly higher in *Eed*<sup>-/-</sup> blastocysts compared to *Eed*<sup>fl/-</sup> (p=0.72) or *Eed*<sup>fl/fl</sup> (p=0.76) female embryos (Figure 3B and Figure 3- figure supplement 1B; Supplementary File 2 and Supplementary File 3). X-linked genes were expressed predominantly from the maternal allele in all three genotypes. Thus, the ratio of maternal:paternal X-linked gene expression in *Eed*<sup>-/-</sup> female blastocysts was broadly similar to that in *Eed*<sup>fl/fl</sup> and *Eed*<sup>fl/-</sup> embryos.

We next sought to validate the RNA-Seq data via Pyrosequencing. Pyrosequencing is a low-throughput technique that can accurately capture allelic expression ratios of individual genes (Cloutier et al., 2018; Gayen, Maclary, Buttigieg, Hinten, & Kalantry, 2015). We analyzed the expression of *Xist* and three X-linked genes subject to X-inactivation, *Rnf12*, *Atrx*, and *Pgk1*.

*Xist* expression analysis by Pyrosequencing was especially important, as there was variability in *Xist* SNP-overlapping read coverage in the RNA-Seq data due potentially to the highly repetitive sequence of *Xist* RNA. We did not detect any significant changes in maternal:paternal allelic expression in hybrid *Eed*<sup>+/-</sup> vs. *Eed*<sup>fl/fl</sup> and *Eed*<sup>fl/-</sup> blastocysts (Figure 3C and Figure 3- figure supplement 1C; Supplementary File 4). Whereas *Xist* was expressed predominantly from the paternal allele, *Rnf12*, *Atrx*, and *Pgk1* were preferentially expressed from the maternal allele in all three genotypes.

As an independent validation of the RNA-Seq and Pyrosequencing results, we also performed RNA FISH to test *Xist* RNA coating and nascent RNA expression of *Rnf12* in *Eed*<sup>+/-</sup> and *Eed*<sup>fl/fl</sup> female (Figure 3D) and male (Figure 3- figure supplement 1D) blastocysts. RNA FISH has the added benefit of providing single cell expression resolution in embryos (Cloutier et al., 2018; Hinten et al., 2016). We distinguished *Eed*<sup>fl/fl</sup> from *Eed*<sup>+/-</sup> female embryos by assaying H3K27me3 enrichment by IF on the *Xist* RNA-coated X-chromosome (Figures 3D and 3E). We classified embryos displaying fewer than 5% of the nuclei with this H3K27me3 enrichment as *Eed*<sup>+/-</sup> (Figure 3E). *Xist* RNA coating and *Rnf12* expression in female *Eed*<sup>+/-</sup> embryos did not differ significantly from *Eed*<sup>fl/fl</sup> blastocysts (Figures 3D and 3F). Both sets of embryos displayed *Xist* RNA coating of one X-chromosome and *Rnf12* expression from the other X-chromosome in a majority of the cells. Male *Eed*<sup>+/-</sup> or *Eed*<sup>fl/-</sup> embryos also did not differ significantly from *Eed*<sup>fl/fl</sup> embryos in their *Rnf12* expression patterns (Figure 3- figure supplement 1D). Thus, by three independent assays – allele-specific RNA-Seq, Pyrosequencing, and RNA FISH – we found that zygotic *Eed* expression is largely dispensable for the initiation and establishment of imprinted X-inactivation.

### **Defective Imprinted X-inactivation Initiation in *Eed*<sup>m/-</sup> Embryos**

Since early *Eed*<sup>+/-</sup> embryos harbor WT maternally-derived EED protein, we next examined the role of maternal EED in initiating imprinted X-inactivation in *Eed*<sup>m/-</sup> and *Eed*<sup>mz/-</sup> blastocysts,

which are devoid of maternally-derived EED. *Eed*<sup>m-/-</sup> blastocysts exhibited a small percentage of nuclei with H3K27me3 enrichment coinciding with the Xist RNA coat (Figure 4A). *Eed*<sup>mz-/-</sup> blastocysts, on the other hand, lacked all such overlapping accumulation (Figure 4A). H3K27me3 enrichment on the Xist RNA-coated X-chromosome in *Eed*<sup>m-/-</sup> but not *Eed*<sup>mz-/-</sup> blastocysts is likely due to the expression of zygotic *Eed* in *Eed*<sup>m-/-</sup> but not *Eed*<sup>mz-/-</sup> embryos (Figure 2).

To test if maternal EED regulates imprinted X-inactivation, we conducted allele-specific RNA-Seq on individual hybrid *Eed*<sup>m-/-</sup> and *Eed*<sup>mz-/-</sup> E3.5 blastocysts (Figure 4- figure supplement 1A). Strikingly, the RNA-Seq data revealed a relative increase in paternal X-linked gene expression in *Eed*<sup>m-/-</sup> and *Eed*<sup>mz-/-</sup> embryos compared to *Eed*<sup>fl/fl</sup>, *Eed*<sup>fl/-</sup>, and *Eed*<sup>+/-</sup> embryos (Figures 4B, 4C, and Figure 4- figure supplement 1B; Supplementary File 2 and Supplementary File 3). Furthermore, *Eed*<sup>mz-/-</sup> embryos appeared to express paternal X-linked genes to a greater degree compared to *Eed*<sup>m-/-</sup> embryos (Figure 4B). When allelic expression ratios of all X-linked genes in Figure 4B were averaged, however, the difference between *Eed*<sup>m-/-</sup> and *Eed*<sup>mz-/-</sup> embryos did not reach statistical significance (p=0.14) (Figure 4C; Supplementary File 3).

The shift in the ratio of X-linked gene expression towards the paternal allele in *Eed*<sup>m-/-</sup> and *Eed*<sup>mz-/-</sup> embryos could be due to increased paternal X-linked gene expression or to decreased maternal X-linked gene expression. To determine the source of the expression change, we calculated the normalized expression of genes on the maternal and paternal X-chromosomes for all genotypes (Figure 4D and Figure 4- figure supplement 1C). Whereas paternal X-linked genes significantly increased in expression, maternal X-linked gene expression decreased in *Eed*<sup>m-/-</sup> and *Eed*<sup>mz-/-</sup> embryos compared to *Eed*<sup>fl/fl</sup>, *Eed*<sup>fl/-</sup>, and *Eed*<sup>+/-</sup> embryos. The increase in paternal X-linked gene expression in *Eed*<sup>m-/-</sup> and *Eed*<sup>mz-/-</sup> embryos was significant when compared to the three other genotypes. The decrease in maternal X-linked gene expression in *Eed*<sup>m-/-</sup> and *Eed*<sup>mz-/-</sup> embryos reached significance only vs. *Eed*<sup>fl/fl</sup> embryos and not vs. *Eed*<sup>fl/-</sup> and



*Eed*<sup>f/-</sup> embryos. The lack of a significant decrease between *Eed*<sup>m/-</sup> and *Eed*<sup>mz/-</sup> embryos compared to *Eed*<sup>fl/-</sup> and *Eed*<sup>f/-</sup> embryos is likely due to the greater variation in maternal X-linked gene expression in *Eed*<sup>fl/-</sup> and *Eed*<sup>f/-</sup> embryos (Supplementary File 3). Finally, *Eed*<sup>mz/-</sup> embryos displayed a significant increase in paternal X-linked gene expression compared to *Eed*<sup>m/-</sup> embryos (p=0.02; Supplementary File 2 and Supplementary File 3), suggesting that zygotic EED can contribute to the silencing of a subset of X-linked genes in blastocysts.

To validate the *Eed*<sup>m/-</sup> and *Eed*<sup>mz/-</sup> blastocyst RNA-Seq data, we again analyzed allele-specific expression of *Xist*, *Rnf12*, *Atrx*, and *Pgk1* in E3.5 blastocysts by Pyrosequencing. Pyrosequencing also showed a significant defect in the initiation and establishment of imprinted X-inactivation in *Eed*<sup>m/-</sup> and *Eed*<sup>mz/-</sup> embryos (Figure 4E and Figure 4- figure supplement 1D; Supplementary File 4). In *Eed*<sup>m/-</sup> and *Eed*<sup>mz/-</sup> embryos, *Xist* expression unexpectedly increased from the maternal-X relative to the paternal-X. Conversely, the expression of *Rnf12* and *Atrx* increased from the paternal-X relative to the maternal-X in *Eed*<sup>m/-</sup> embryos. In *Eed*<sup>mz/-</sup> embryos, in addition to *Rnf12* and *Atrx*, *Pgk1* also displayed nearly equal levels of expression from the maternal and paternal alleles. The Pyrosequencing results thus recapitulate the defects in imprinted X-inactivation observed by RNA-Seq.

Together, the RNA-Seq and Pyrosequencing data lead to several suggestions. The first is that maternal EED depletion induces *Xist* from the maternal X-chromosome in the early embryo. This derepression is consistent with maternally-derived PRC2 repressing the maternal *Xist* locus, which is marked by H3K27me3 in the oocyte [Figure 4- figure supplement 1E; (Zheng et al., 2016)]. Ectopic *Xist* induction from the maternal-X then results in the silencing of genes on that X-chromosome. The second major suggestion is that loss of maternal EED induces paternal X-linked genes. Finally, the data implicate zygotic EED expression in the silencing of a subset of paternal X-linked genes at the onset of imprinted X-inactivation.

## **Maternal EED Silences *Xist* on the Maternal-X**

To validate the RNA-Seq and Pyrosequencing data from the maternal *Eed* mutants, we performed RNA FISH in *Eed*<sup>m-/-</sup> and *Eed*<sup>mz-/-</sup> blastocysts for *Xist* and *Rnf12* (Figure 5A). Whereas most nuclei in *Eed*<sup>m-/-</sup> and *Eed*<sup>mz-/-</sup> females displayed a single Xist RNA coat and monoallelic expression of *Rnf12*, a subset displayed Xist RNA coating of both X-chromosomes. The majority of these nuclei also lacked *Rnf12* expression, suggesting silencing of *Rnf12* on both X-chromosomes.

We similarly examined *Eed*<sup>mz-/-</sup> male blastocysts (Figure 5B). A subset of nuclei in *Eed*<sup>mz-/-</sup> male mutant embryos also exhibited ectopic Xist RNA coating of their sole, maternal X-chromosome. Interestingly, *Eed*<sup>mz-/-</sup> male embryos were present in two distinct morphological classes. The first category was comprised of large, well-developed embryos, which displayed few or no nuclei with Xist RNA coating. The second category consisted of underdeveloped embryos, which displayed Xist RNA-coating in much higher proportions (20-60% of nuclei). In both sets of embryos, Xist RNA coating was often accompanied by a loss of *Rnf12* expression from the X-chromosome. These data suggest that Xist RNA coating hinders developmental progression by silencing genes on the ectopically Xist RNA-coated X-chromosome. *Eed*<sup>mz-/-</sup> embryos that adaptively repress *Xist* may overcome this developmental deficiency.

The correlation between reduced frequency of ectopic Xist RNA-coated nuclei and development of *Eed*<sup>mz-/-</sup> embryos led us to test the developmental competency of maternal-null *Eed* embryos. We assessed if *Eed*<sup>m-/-</sup> embryos could yield live born animals. To our surprise, a small number of *Eed*<sup>m-/-</sup> female as well as male embryos could live to term (Figure 5C), suggesting that the ectopic Xist RNA expression and coating could be resolved in maternal-null embryos of both sexes. Interestingly, significantly more females were born compared to males (p=0.02, Two-tailed Student's T-test), suggesting that females can more robustly extinguish ectopic Xist RNA expression compared to males. These data further suggest that zygotic EED expression is sufficient to compensate for the absence of maternal EED in a subset of the early

embryos. *Eed*<sup>mz/-</sup> embryos are expected to be inviable, since loss of zygotic *Eed* expression results in lethality of both female and male embryos (Faust, Schumacher, Holdener, & Magnuson, 1995; Shumacher et al., 1996; J. Wang et al., 2001).

### **Switching of Imprinted to Random X-inactivation in *Eed*<sup>m/-</sup> Embryos**

The relative paucity of ectopic Xist RNA-coated nuclei in female *Eed*<sup>m/-</sup> and *Eed*<sup>mz/-</sup> blastocysts observed by RNA FISH in Figure 5A-B is inconsistent with the robust ectopic Xist RNA expression from and silencing of maternal X-linked genes and the increased expression of paternal X-linked genes that are detected via Pyrosequencing and RNA-Seq (Figure 4B-D). We thus postulated that instead of undergoing imprinted inactivation of the paternal X-chromosome, *Eed*<sup>m/-</sup> and *Eed*<sup>mz/-</sup> blastocysts switch to random X-inactivation of either the maternal- or the paternal-X in individual cells. Such mosaicism would explain the silencing of maternal X-linked genes and the induction of paternal X-linked gene expression in *Eed*<sup>m/-</sup> and *Eed*<sup>mz/-</sup> female embryos detected by RNA-Seq and Pyrosequencing.

To test the above model of X-inactivation mosaicism, we developed and applied an allele-specific Xist RNA FISH strategy on hybrid control *Eed*<sup>fl/+</sup> and test *Eed*<sup>m/-</sup> female E3.5 blastocysts (Materials and Methods; Figure 6- figure supplement 1). Allele-specific Xist RNA FISH allowed us to discriminate Xist RNA expression from the maternal vs. the paternal X-chromosome in individual cells. Allele-specific Xist RNA FISH displayed Xist RNA expression from the paternal-X in *Eed*<sup>fl/+</sup> female blastocysts (Figure 6A), as would be expected from embryos stably undergoing imprinted X-inactivation of the paternal-X. In *Eed*<sup>m/-</sup> female blastocysts, we saw a mosaic distribution of Xist RNA expression and coating. Whereas some *Eed*<sup>m/-</sup> blastocyst nuclei displayed Xist RNA expression from and coating of the maternal-X, others exhibited Xist RNA expression from and coating of the paternal-X. A subset of nuclei in *Eed*<sup>m/-</sup> blastocysts exhibited Xist RNA expression from both the maternal and paternal X-chromosomes (Figure 6A), consistent with the non-allele specific Xist RNA FISH data from *Eed*<sup>m/-</sup> and *Eed*<sup>mz/-</sup>

blastocysts in Figure 5A. Male *Eed<sup>m/-</sup>* embryos similarly displayed ectopic Xist RNA expression from and coating of their sole maternally-inherited X-chromosome in approximately 50% of nuclei (Figure 6B).

From the blastocyst data, we extrapolated that earlier *Eed<sup>m/-</sup>* embryos may harbor a higher proportion of cells with ectopic Xist RNA coating of the maternal-X. This pattern is later resolved into the mosaic Xist RNA coating pattern observed at the blastocyst stage in females and loss of the Xist RNA coat in males. We therefore performed allele-specific Xist RNA FISH on 3-16 cell control *Eed<sup>fl/+</sup>* and test *Eed<sup>m/-</sup>* hybrid embryos. In the *Eed<sup>fl/+</sup>* female embryos, Xist RNA was expressed from and coated only the paternal X-chromosome (Figure 7A). Most *Eed<sup>m/-</sup>* female embryos, by contrast, displayed a high percentage of nuclei with Xist RNA expression and coating of both X-chromosomes (Figure 7A). In male 3-17 cell embryos, *Eed<sup>fl/+</sup>* embryos did not show any nuclei with Xist RNA coating (Figure 7B). In *Eed<sup>m/-</sup>* male embryos, by contrast, almost every nucleus exhibited ectopic Xist expression from and coating of the maternally-inherited X-chromosome (Figure 7B). Thus, in the absence of maternal EED most cells express Xist from both X-chromosomes in early female embryos and from the sole X in early male embryos. By the blastocyst stage, however, one of the two Xist alleles is stochastically silenced in most female cells and the sole Xist allele is silenced in most male cells.

### **Lack of Maternal EED in Human Embryos**

Intriguingly, the Xist RNA coating of both X-chromosomes in female and of the single X in male early preimplantation *Eed<sup>m/-</sup>* and *Eed<sup>mz/-</sup>* embryos resemble the pattern observed in preimplantation human female and male embryos (Okamoto et al.; Petropoulos et al., 2016). In early preimplantation human embryos, females display Xist RNA coating of both Xs and males of their sole maternally-inherited X. We therefore hypothesized that the Xist RNA expression profile in early human embryos may reflect the absence of maternally-derived EED and other

core PRC2 proteins in human oocytes. To test this hypothesis, we analyzed RNA-Seq data from mouse and human oocytes to determine the expression levels of core PRC2 genes *Eed*, *Ezh2*, *Ezh1*, and *Suz12* (Kobayashi et al., 2012; Macfarlan et al., 2012; Reich, Klatsky, Carson, & Wessel, 2011). Compared to mouse oocytes, human oocytes expressed all four genes at negligible levels (Figure 8A). This difference in the expression of PRC2 components in oocytes may underlie why early mouse but not human embryos undergo imprinted X-inactivation.

## **Discussion**

Genomic imprinting is a paradigm of transgenerational epigenetic inheritance, since the two parental alleles undergo diametrically divergent transcriptional fates in the embryo. Imprinted X-inactivation is an extreme example of genomic imprinting in that most genes on the paternally-inherited X-chromosome undergo silencing. The maternal X-chromosome, by contrast, remains active. Here, we define the transition of maternal to zygotic EED expression in the early embryo and find the presence of maternal but not zygotic EED when imprinted X-inactivation begins. Upon ablation of *Eed* in the oocyte and the absence of maternally-derived EED in the embryo, the initiation of imprinted X-inactivation is compromised (Figure 8B). Maternal-null (*Eed*<sup>m-/-</sup> and *Eed*<sup>mz-/-</sup>) but not zygotic-null (*Eed*<sup>-/-</sup>) early preimplantation female and male embryos ectopically induce Xist RNA from the maternal X-chromosome. Early *Eed*<sup>m-/-</sup> female embryos therefore display Xist RNA-coating of both X-chromosomes and mutant males of the sole maternally-inherited X-chromosome.

PRC2-catalyzed H3K27me3 marks the *Xist* locus on the maternal X-chromosome during oogenesis (Zheng et al., 2016). In agreement, the injection of the H3K27me3 demethylase *Kdm6b* in the zygote resulted in the derepression of the *Xist* locus on the maternal X-chromosome in 8-16 cell embryos (Inoue, Jiang, Lu, & Zhang, 2017). Female morulas derived from *Kdm6b*-injected zygotes displayed Xist RNA coating of both the maternal and the paternal X-chromosome in most blastomeres, suggesting inactivation of both Xs in the embryo.

351 Nullizygosity of X-linked gene expression due to inactivation of both Xs in females or of the  
352 single-X in males is expected to result in cell and embryo lethality (Gayen et al., 2015). The  
353 conditional deletion of *Eed* in the oocyte, however, yielded live born mice, implying that ectopic  
354 *Xist* expression due to H3K27me3 loss and the ensuing inactivation of the maternal-X in the  
355 early embryo is resolved later [this study; (Prokopuk et al., 2018)]. In agreement, our study  
356 shows that by the blastocyst stage most nuclei in *Eed*<sup>m-/-</sup> and *Eed*<sup>mz-/-</sup> female embryos exhibit  
357 only one Xist RNA coat. However, instead of Xist RNA coating exclusively of the paternal X-  
358 chromosome as in WT embryos, the maternal *Eed* mutants express Xist RNA from and coat  
359 either the maternal or the paternal X-chromosome, a hallmark of random X-inactivation. This  
360 randomization persists later in development in extraembryonic tissues (data not shown), which  
361 normally maintain imprinted inactivation of the paternal-X. Like *Eed*<sup>m-/-</sup> and *Eed*<sup>mz-/-</sup> females,  
362 *Eed*<sup>m-/-</sup> and *Eed*<sup>mz-/-</sup> male blastocysts also extinguish ectopic *Xist* induction.

363 In addition to maternal EED, our data argue that zygotically generated EED contributes to  
364 imprinted X-inactivation in the early embryo. In comparison to *Eed*<sup>m-/-</sup> embryos, *Eed*<sup>mz-/-</sup> female  
365 blastocysts displayed a further increase in paternal X-linked gene expression. One  
366 interpretation of these data is that the onset of zygotic EED expression results in the preferential  
367 installation of H3K27me3 at the *Xist* locus on the maternal-X in some cells of early *Eed*<sup>m-/-</sup>  
368 embryos. These cells thus forestall or extinguish *Xist* expression from the maternal X-  
369 chromosome and inactivate the paternal-X, ultimately resulting in more cells in the embryo in  
370 which the paternal-X is inactive compared to the maternal-X. Loss of both maternal and zygotic  
371 EED would annul such biased inactivation of the paternal-X and thereby cause a greater  
372 increase in paternal X-linked gene expression in *Eed*<sup>mz-/-</sup> embryos. An alternative possibility is  
373 that zygotic EED functions to maintain silencing preferentially of paternal X-linked genes in the  
374 early embryo. The differential sensitivity of genes on the maternal vs. paternal X-chromosomes  
375 to zygotic EED in *Eed*<sup>m-/-</sup> embryos may reflect the different kinetics of inactivation of the two X-

376 chromosomes. The ectopic induction of *Xist* and X-linked gene silencing on the maternal-X may  
377 occur more slowly compared to that on the paternal-X. Due to this delay, genes on the  
378 maternal-X would still be in the process of undergoing silencing in *Eed<sup>mz/-</sup>* blastocysts. A subset  
379 of paternal X-linked genes, on the other hand, may have established silencing and are now in  
380 the maintenance phase of X-inactivation in the blastocysts. In the absence of both maternal  
381 and zygotic EED, then, *Eed<sup>mz/-</sup>* blastocysts fail to maintain silencing of these paternal X-linked  
382 genes. Previous work has shown that zygotic EED is in fact required to maintain silencing of a  
383 discrete set of paternal X-linked genes during imprinted X-inactivation (Kalantry & Magnuson,  
384 2006; Kalantry et al., 2006; Maclary et al., 2017).

385       The ability of the cells of early *Eed<sup>mz/-</sup>* and *Eed<sup>mz/-</sup>* embryos to resolve Xist RNA coating of  
386 both Xs in females or of the single X in males implies that the early embryo has an X-  
387 chromosome counting mechanism that ensures that a single X-chromosome remain active in  
388 females as well as in males, irrespective of its parent of origin. Such a counting mechanism has  
389 previously been proposed by Takagi and colleagues to explain the kinetics of Xist RNA  
390 induction in XX and XY androgenetic embryos, which harbor only paternal X-chromosomes  
391 (Okamoto, Tan, & Takagi, 2000). Like in *Eed<sup>mz/-</sup>* embryos, androgenetic 4 and 8-16 cell  
392 embryos also initially induce Xist RNA from all Xs, which is resolved at the blastocyst stage and  
393 results in females displaying a single Xist RNA coat in most nuclei and males exhibiting few or  
394 no nuclei with Xist RNA coating (Okamoto et al., 2000). Molecular sensing of the X-  
395 chromosomal complement in imprinted X-inactivation is also suggested by studies of diploid XX  
396 parthenogenetic or gynogenetic embryos, which harbor two maternal X-chromosomes. In these  
397 preimplantation bi-maternal XX embryos, *Xist* expression is delayed and appears to occur  
398 stochastically from one or the other X-chromosome (Kay et al., 1994). In agreement, the  
399 extraembryonic tissues of post-implantation XX parthenogenotes display hallmarks of random  
400 X-inactivation instead of the imprinted form observed in WT extraembryonic cells (Rastan,

Kaufman, Handyside, & Lyon, 1980). Randomization of X-inactivation in extraembryonic cells of mouse embryos with two paternal or maternal X-chromosomes led Takagi and colleagues to suggest that imprinted X-inactivation in placental mammals may have arisen from random X-inactivation (Matsui, Goto, & Takagi, 2001), a notion that our data from *Eed*<sup>m-/-</sup> and *Eed*<sup>mz-/-</sup> embryos agree with.

Evidence suggests that the X-linked *Rnf12* gene may be a key component of the X-chromosome counting mechanism during imprinted X-inactivation. The maternal-X allele of *Rnf12* is required to induce *Xist* from the paternal-X in preimplantation mouse embryos (Shin et al., 2010). Upon *Xist* RNA coating, *Rnf12* is rapidly silenced on the paternal X-chromosome (Kalantry et al., 2009; Namekawa et al., 2010; Patrat et al., 2009). In *Eed*<sup>m-/-</sup> and *Eed*<sup>mz-/-</sup> embryos, in addition to the paternal *Rnf12* allele, the maternal *Rnf12* allele is also stringently silenced due to ectopic *Xist* RNA coating of the maternal-X. Since *Rnf12* is required for *Xist* RNA induction in the preimplantation embryo, the silencing of all *Rnf12* alleles in *Eed*<sup>m-/-</sup> and *Eed*<sup>mz-/-</sup> female and male embryos may paradoxically lead to the loss of *Xist* RNA expression from both Xs in females or from the sole X-chromosome in males. In females, this transient state of two active-Xs may then be followed by random X-inactivation, analogously to how differentiating pluripotent epiblast cells undergo random X-inactivation (Gayen et al., 2015; Maclary et al., 2014; Mak et al., 2004). The X-chromosome counting process and randomization of X-inactivation in the early embryo may explain how *Eed*<sup>m-/-</sup> embryos can yield live born animals [this study and (Prokopuk et al., 2018)].

In the course of preparing this manuscript, a publication reported that extraembryonic tissues of *Eed* maternal-null female post-implantation embryos exhibit random X-inactivation (Inoue, Chen, Yin, & Zhang, 2018). The primary piece of data in the study supporting this conclusion is the expression of maternal and paternal X-linked genes, including *Xist*, in post-implantation E6.5 female *Eed*<sup>m-/-</sup> extraembryonic tissues by allele-specific RNA-Seq. Although



in agreement with our conclusions, the study does not directly demonstrate when imprinted X-inactivation switches to random X-inactivation and whether loss of zygotic *Eed* would result in a similar outcome. Our study, by contrast, genetically dissects the relative contributions of maternal vs. zygotic EED in the initiation and establishment of imprinted X-inactivation by three different approaches, allele-specific RNA-Seq, Pyrosequencing, and allele-specific Xist RNA FISH. We are thus able to pinpoint when and how the loss of maternal EED converts imprinted X-inactivation to random X-inactivation in preimplantation embryos. Genetically testing the requirement of maternal vs. zygotic EED is necessary to determine that the establishment of imprinted X-inactivation in the preimplantation embryo is maternally but not zygotically controlled.

Xist RNA expression in *Eed*<sup>m-/-</sup> mouse embryos mimics the pattern observed in human embryos, which do not undergo imprinted X-inactivation and ultimately display only random X-inactivation (Okamoto et al.; Petropoulos et al., 2016). In agreement, like the *Eed*<sup>m-/-</sup> and *Eed*<sup>mz-/-</sup> embryos, human oocytes do not express *Eed* and other core PRC2 genes, suggesting that the presence or absence of maternal PRC2 proteins may dictate whether placental mammals undergo imprinted X-inactivation.

## Acknowledgments

We thank Paul Ginart and Arjun Raj for help with designing of the allele-specific Xist RNA FISH assay. We also thank Milan Samanta for isolating a subset of the mouse embryos; Emily Maclary for establishing the allele-specific RNA-Seq pipeline used in the study and initiating the RNA-Seq analysis of embryos. We thank Gregory Myers for critically evaluating the manuscript. We acknowledge the services of the University of Michigan Sequencing Core Facility, supported in part by the University of Michigan Comprehensive Cancer Center; and, the University of Michigan Transgenic Animal Model Core. This work was funded by NIH Institutional National Research Service Awards T32-GM07544 (University of Michigan

Predoctoral Genetics Training Program; to M.C. and M.T.), an NIH Director's New Innovator Award (DP2-OD-008646) (to S.K.), a March of Dimes Basil O'Connor Starter Scholar Research Award (5-FY12-119) (to S.K.), an NIH NIGMS R01 Award (R01GM124571) (to S.K.), NIH NICHD R01 Award (R01HD095463) (to S.K.), and the University of Michigan Endowment for the Basic Sciences (S.K.). Sequencing data generated for this study have been submitted to the NCBI Gene Expression Omnibus (GEO; <http://www.ncbi.nlm.nih.gov/geo/>) under accession number GSE123173.

**Competing Interests**

All authors have no financial or non-financial competing interests with this study or its publication.

476

477

478 **Materials and Methods**

Reagent type (species) or resource	Designation	Source or reference	Identifiers	Additional information
gene ( <i>Mus</i> )	<i>Eed</i>	ENSEMBL	ENSEMBL:ENSMUSG0000030619	Chromosome 7: 89,954,654-89,980,983 reverse strand
strain, strain background ( <i>Mus molossinus</i> )	JF1/Ms; <i>Mus molossinus</i>	JAX	JAX:003720; RRID:MGI:2164136	
strain, strain background ( <i>Mus musculus</i> )	129/S1; <i>Mus musculus</i>	JAX	JAX:002448	
genetic reagent ( <i>Protamine-cre</i> )	<i>Prm-cre</i>	O'Gorman et al., 1997 (PMID: 9405659); JAX	JAX:003328	
genetic reagent ( <i>Zp3-cre</i> )	<i>Zp3-cre</i>	Lewandoski et al., 1997 (PMID: 9016703); JAX	JAX:003651	
biological sample (mouse embryo)	<i>Mus musculus</i> ; <i>Mus molossinus</i>	this paper		2 cell stage to blastocyst stage embryos
biological sample (RNA)	<i>Mus musculus</i> ; <i>Mus molossinus</i>	this paper		Generated from female blastocysts
antibody	Monoclonal EED (Rabbit monoclonal)	Sewalt et al., 1998 (PMID: 9584199)		Obtained from Otte Lab; Dilution: Figure 1 - 1:1000, Figure 2 - 1:2500
antibody	Polyclonal H3K27me3 (Rabbit polyclonal)	Millipore	Millipore:#ABE44	Dilution: Figure 1 - 1:5000, Figure 2 - 1:25000
antibody	Alexa Fluor DaM 555 (secondaries)	Invitrogen	Invitrogen:#A32773	Dilution: Figure 1 - 1:300, Figure 2 - 1:500
antibody	Alexa Fluor DaRb 488 (secondaries)	Invitrogen	Invitrogen:#A21206	Dilution: Figure 1 - 1:300, Figure 2 - 1:500
antibody	Alexa Fluor DaRb 647 (secondaries)	Invitrogen	Invitrogen:#A31573	Dilution: 1:300
sequence-based reagent	Quasar dye 570	Biosearch Technologies	primer sequences in Supplemental File 5	Allele specific probe dye; labeled <i>M. musculus</i> -specific oligo
sequence-based reagent	Quasar dye g70	Biosearch Technologies	primer sequences in Supplemental File 5	Allele specific probe dye; labeled <i>M. molossinus</i> -specific oligo
commercial assay or kit	Dynabeads mRNA DIRECT Kit	Thermo Fisher	ThermoFisher:#610.11	
commercial assay or kit	Takara SMARTer Seq V4 stranded low input kit	Takara	Takara:#634889	
commercial assay or kit	BioPrime DNA Labeling System	Invitrogen	Invitrogen:#18094011	
software, algorithm	FastQC	<a href="http://www.bioinformatics.babraham.ac.uk/projects/fastqc">http://www.bioinformatics.babraham.ac.uk/projects/fastqc</a>	RRID:SCR_014583	
software, algorithm	R	<a href="https://www.r-project.org">https://www.r-project.org</a>	RRID:SCR_001905	Used in RNA-Seq analysis
software, algorithm	VCFtools	Danecek et al., 2011 (PMID: 21653522)	RRID:SCR_001235	Used in RNA-Seq analysis
software, algorithm	STAR	Dobin et al., 2013 (PMID: 23104886)	RRID:SCR_015899	Used in RNA-Seq analysis

software, algorithm	HTSeq	Anders et al., 2015 (PMID: 25260700)	RRID:SCR_005514	Used in RNA-Seq analysis
software, algorithm	FeatureCounts	Liao et al., 2014 (PMID: 24227677)	RRID:SCR_012919	Used in RNA-Seq analysis
other	DAPI stain	Invitrogen	Invitrogen:#D21490	Dilution: 1:250,000
other	Cy3-dCTP	GE Healthcare	GEHealthcare:#PA53021	
other	Fluorescein-12-UTP	Roche	Roche:#11427857910	
other	Cy5-CTP	GE Healthcare	GEHealthcare:#25801087	
other	SSC	Ambion	Ambion:#AM9765	RNA FISH hybridization buffer; Working concentration: 4X AISP working concentration: 2X
other	Dextrane sulfate	Millipore	Millipore:#S4030	RNA FISH hybridization buffer; Working concentration: 20% AISP working concentration: 10%
other	Formamide, deionized	VWR Life Sciences	VWR:#0606	RNA FISH hybridization buffer; AISP working concentration: 10%
other	BSA	New England Biolabs	NEB:#B9001S	IF blocking buffer; Working concentration: 0.5 mg/ml
other	yeast tRNA	Invitrogen	Invitrogen:#15401-029	IF blocking buffer; Working concentration: 50 ug/ml
other	RNAase out	Invitrogen	Invitrogen:#10777-019	IF blocking buffer; Working concentration: 80 units/ml
other	Tween-20	Thermo Fisher	ThermoFisher:#BP337-100	IF blocking buffer; Working concentration: 0.2%
other	PBS	Gibco	Gibco:#14200	IF blocking buffer; Working concentration: 1X
other	Vectashield	Vector Labs	VectorLabs: #H-1000	plating medium

## Ethics Statement

This study was performed in strict accordance with the recommendations in the Guide for the Care and Use of Laboratory Animals of the National Institutes of Health. All animals were handled according to protocols approved by the University Committee on Use and Care of Animals (UCUCA) at the University of Michigan (protocol #s PRO6455 and PRO8425).

## Mice

Mice harboring a conditional mutation in *Eed* were described in our prior publication (Maclary et al., 2017). A *Mus molossinus* JF1 X-chromosome was introgressed to generate *Eed*<sup>fl/fl</sup>; X<sup>JF1</sup> Y males. *Mus musculus* *Eed*<sup>fl/fl</sup> females were backcrossed onto the 129/S1 background. The X-linked *Gfp* transgenic (X-*Gfp*) and JF1 strains have been described previously (Hadjantonakis, Gertsenstein, Ikawa, Okabe, & Nagy, 1998; Kalantry & Magnuson, 2006; Kalantry et al., 2006; Kalantry et al., 2009; Maclary et al., 2017).

Embryos generated for the purpose of allele-specific RNA-Seq, Pyrosequencing, or allele-specific RNA fluorescence *in situ* hybridization (FISH) were sired by males harboring the X<sup>JF1</sup> X-chromosome. Embryos generated for immunofluorescence (IF) and non-allele specific RNA

FISH were sired by males harboring the *X-Gfp* transgene. The paternal *X-Gfp* is only transmitted to daughters. Thus, GFP fluorescence conferred by the paternally-transmitted *X-Gfp* transgene was used to sex the embryos.

For derivation of embryos lacking zygotic *Eed*, the *Protamine-Cre* (*Prm-Cre*) transgene was bred into an *Eed<sup>fl/fl</sup>* or *Eed<sup>fl/-</sup>* background. *Prm-Cre* is expressed only during spermatogenesis (O'Gorman et al., 1997), thus resulting in the deletion of the *Eed* floxed allele in the male germline. For derivation of embryos lacking maternal *EED*, a *Cre* transgene controlled by the *Zona pellucida 3* gene promoter (*Zp3-Cre*) (Lewandoski et al., 1997), was used to delete the floxed *Eed* alleles in growing oocytes.

## Mouse Embryo Dissections and Processing

E3.5 embryos were isolated essentially as described (Maclary et al., 2014). Embryos were flushed from the uterine limbs in 1X PBS (Invitrogen, #14200) containing 6 mg/ml BSA (Invitrogen, #15260037).

Two to sixteen cell embryos were flushed from oviducts of superovulated females with 1X PBS (Invitrogen, #14200) containing 6 mg/ml BSA (Invitrogen, #15260037). For superovulation, 4-5-week-old, or 9-12-week-old females were treated with 5 IU of pregnant mare's serum gonadotropin (PMSG, Sigma, # G-4877) and 46 hours later with 5 IU of human chorionic gonadotropin (hCG, Sigma, #CG-5). Embryos were harvested 48-74 hours post hCG.

The zona pellucida surrounding embryos was removed through incubation in cold acidic Tyrode's solution (Sigma, #T1788), followed by neutralization through several transfers of cold M2 medium (Sigma, #M7167).

Isolated E3.5 embryos were either lysed for RNA isolation or plated onto 0.2% gelatin- (Sigma, #G2500) and/or 0.01% Poly-L-Lysine (PLL, Sigma # P4707)-coated glass coverslips in 0.25X PBS for immunofluorescence (IF) coupled with RNA *in situ* hybridization (FISH). 2-16 cell embryos were plated on coverslips coated in 0.01% Poly-L-Lysine for IF. E3.5 or 4-16 cell embryos were plated on coverslips coated with 1X Denhardt's (Sigma, #D9905) solution for allele-specific RNA FISH. For plated embryos, excess solution was aspirated, and coverslips were air-dried for approximately 15-30 mins. After drying, embryos were permeabilized and fixed in 50  $\mu$ L solution of either 0.05% or 0.1% Tergitol (Sigma, #NP407) with 1% paraformaldehyde (Electron Microscopy Sciences, #15710) in 1X PBS for 5 min, followed by 1% paraformaldehyde in 1X PBS for an additional 5 min. Excess solution was tapped off onto paper towels, and coverslips were rinsed 3X with 70% ethanol and stored in 70% ethanol at -20°C prior to IF or RNA FISH.

## PCR

For embryo DNA isolation, embryos were isolated as described above, individual blastocysts were lysed in 15  $\mu$ L buffer composed of 50 mM KCl, 10 mM Tris-Cl (pH 8.3), 2.5 mM MgCl<sub>2</sub>, 0.1 mg/mL gelatin, 0.45% NP-40, 0.45% Tween-20, and 0.4 mg/mL Proteinase K (Fisher, #BP1700). Embryos in lysis buffer were incubated at 50°C overnight, then stored at 4°C until use. Genomic PCR used 1-3  $\mu$ L lysate per sample. Reactions for *Eed* were carried out in ChromaTaq buffer (Denville Scientific) with 2.5 mM MgCl<sub>2</sub> added. XX vs. XY sexing PCR reactions were carried out in Klennterm buffer (670mM Tris pH 9.1, 160mM (NH<sub>4</sub>)SO<sub>4</sub>, 35mM MgCl<sub>2</sub>, 15mg/ml BSA). Both used RadiantTaq DNA polymerase (Alkali Scientific, #C109). Primer sequences are described in Supplementary File 5.

Liveborn animals from the cross of *Eed<sup>fl/fl</sup>;Zp3-Cre* female by WT male were genotyped for *Eed* to confirm deletion of the floxed allele. Ear punches were taken after weaning and lysed in 50  $\mu$ L of lysis buffer (above). Ear punches were incubated at 50°C overnight, then stored at 4°C until use. 1  $\mu$ L of DNA lysate was used per reaction. *Eed* PCRs were carried out as above.

### Quantification of Allele-specific Expression by Pyrosequencing

Allele-specific expression was quantified using the Qiagen PyroMark sequencing platform, as previously described (Gayen et al., 2015). Briefly, the amplicons containing SNPs were designed using the PyroMark Assay Design software. cDNAs were synthesized using Invitrogen SuperScript III One-Step RT-PCR System (Invitrogen, #12574-026). Following the PCR reaction, 5  $\mu$ L of the 25  $\mu$ L reaction was run on a 3% agarose gel to assess the efficacy of amplification. The samples were then prepared for pyrosequencing according to the standard recommendations for use with the PyroMark Q96 ID sequencer. All amplicons spanned intron(s), thus permitting discrimination of RNA vs. any contaminating genomic DNA amplification due to size differences. Control reactions lacking reverse transcriptase for each sample were also performed to rule out genomic DNA contamination. E3.5 embryos of similar sizes for all genotypes were used in the Pyrosequencing assays. Pyrosequencing primer sequences are described in Supplementary File 5.

### Immunofluorescence (IF)

Embryos mounted on gelatin-, PLL-, and/or PLL/gelatin-coated glass coverslips were washed 3 times in 1X PBS for 3 min each while shaking. Coverslips were then incubated in blocking buffer consisting of 0.5 mg/mL BSA (New England Biolabs, #B9001S), 50  $\mu$ g/mL yeast tRNA (Invitrogen, #15401-029), 80 units/mL RNaseOUT (Invitrogen, #10777-019), and 0.2% Tween 20 (Fisher, #BP337-100) in 1X PBS in a humid chamber for 30 min at 37°C. The samples were next incubated with primary antibody diluted in blocking buffer for 45 min -2 hr in the humid chamber at 37°C. The samples were then washed 3 times in 1X PBS/0.2% Tween 20 for 3 min each while shaking. After a 5 min incubation in blocking buffer at 37°C in the humid chamber, the samples were incubated in blocking buffer containing fluorescently-conjugated secondary antibody for 30 min in the humid chamber at 37°C, followed by three washes in PBS/0.2% Tween 20 while shaking for 3 min each. For samples undergoing only IF, DAPI was added to the third wash at a 1:250,000 dilution. Coverslips were then mounted on slides in Vectashield (Vector Labs, #H-1000). For samples undergoing IF and RNA FISH, the samples were processed for RNA FISH following the third wash. Antibody information is described in Supplementary File 5.

### RNA Fluorescence *In Situ* Hybridization (RNA FISH)

RNA FISH with double-stranded and strand-specific probes was performed as previously described (Gayen et al., 2015; Hinten et al., 2016; Kalantry et al., 2009). The *Rnf12* dsRNA FISH probe was made by random-priming using BioPrime DNA Labeling System (Invitrogen, #18094011) and labeled with Cy3-dCTP (GE Healthcare, #PA53021) using a previously described fosmid template (Kalantry et al., 2009). Strand-specific *Xist* probes were generated from templates as described (Maclary et al., 2014; Sarkar et al., 2015). Probes were labeled with Fluorescein-12-UTP (Roche, #11427857910) or Cy5-CTP (GE Healthcare, #25801087). Labeled probes from multiple templates were precipitated in a 0.5M ammonium acetate solution (Sigma, #09691) along with 300  $\mu$ g of yeast tRNA (Invitrogen, #15401-029) and 150  $\mu$ g of sheared, boiled salmon sperm DNA (Invitrogen, #15632-011). The solution was then spun at

15,000 rpm for 20 min at 4°C. The pellet was washed consecutively with 70% ethanol and 100% ethanol while spinning at 15,000 rpm at room temperature. The pellet was dried and resuspended in deionized formamide (VWR, #97062-010). The probe was denatured by incubating at 90°C for 10 min followed by an immediate 5 min incubation on ice. A 2X hybridization solution consisting of 4X SSC and 20% Dextran sulfate (Millipore, #S4030) was added to the denatured solution. All probes were stored in the dark at -20°C until use.

Following IF, embryos mounted on coverslips were dehydrated through 2 min incubations in 70%, 85%, 95%, and 100% ethanol solutions and subsequently air-dried. The coverslips were then hybridized to the probe overnight in a humid chamber at 37°C. The samples were then washed 3 times for 7 min each at 37°C with 2X SSC/50% formamide, 2X SSC, and 1X SSC. A 1:250,000 dilution of DAPI (Invitrogen, #D21490) was added to the third 2X SSC wash. Coverslips were then mounted on slides in Vectashield (Vector Labs, #H-1000).

### Allele-specific Xist RNA FISH

Allele specific Xist RNA FISH probes were generated as described (Levesque, Ginart, Wei, & Raj, 2013). Briefly, a panel of short oligonucleotide probes were designed to uniquely detect either the *M. musculus* or the *M. molossinus* alleles of *Xist* (Supplementary File 5). Five probes were designed for each *Xist* allele. Each probe overlapped a SNP that differs between the two strains, with the SNP located at the fifth base pair position from the 5' end. The same panel of five SNPs was used for both sets of allele-specific probes. The 3' end of each oligonucleotide probe is fluorescently tagged using Quasar dyes (Biosearch technologies). *M. musculus*-specific oligos were labeled with Quasar 570 and *M. molossinus* oligos labeled with Quasar 670. In addition to labeled SNP-overlapping oligonucleotides, a panel of 5 "mask" oligonucleotides were also synthesized. These "mask" probes are complimentary to the 3' end of the labeled allele-specific probes and will hybridize to the allele-specific oligonucleotides, leaving only 9-10 base pairs of sequence surrounding the polymorphic site available to initially hybridize to the target Xist RNA. Since this region of complementarity is short, the presence of a single nucleotide polymorphism is sufficient to destabilize the hybridization with the alternate allele. Sequences of detection and mask probes are listed in Supplementary File 5. Allele-specific Xist RNA FISH probes were combined with a strand-specific Xist RNA probe, labeled with Fluorescein-12-UTP (Roche, #11427857910), which served as a guide probe that hybridizes to Xist RNA generated from both *Xist* alleles and ensured the fidelity of the allele-specific probes in detecting the cognate Xist RNA molecules. The guide Xist RNA probe was first ethanol precipitated as previously described, then resuspended in hybridization buffer containing 10% dextran sulfate, 2X saline-sodium citrate (SSC) and 10% formamide. The precipitated guide RNA probe was then mixed with the *M. musculus* and *M. molossinus* detection probes, to a final concentration of 5 nM per allele-specific oligo, and 10 nM mask probe, yielding a 1:1 mask:detection oligonucleotide ratio. Coverslips were hybridized to the combined probe overnight in a humid chamber at 37°C. After overnight hybridization, samples were washed twice in 2X SSC with 10% formamide at 37°C for 30 min, followed by one wash in 2X SSC for 5 mins at room temperature. A 1:250,000 dilution of DAPI (Invitrogen, #D21490) was added to the second 2X SSC with 10% formamide wash. Coverslips were then mounted on slides in Vectashield (Vector Labs, #H-1000).

### Microscopy

Stained samples were imaged using a Nikon Eclipse TiE inverted microscope with a Photometrics CCD camera. The images were deconvolved and uniformly processed using NIS-Elements software. For four color images (blue, green, red, and white), the far-red spectrum



was employed for the fourth color (AlexaFluor 647 secondary antibody and Cy5-UTP labelled riboprobes for RNA FISH). Additional antibody information is outlined in Supplementary File 5.

EED and H3K27me3 IF intensity quantification were performed using the “3D Measurement; 3D thresholding, 3D viewing and voxel based measurements” software package (Nikon Instruments, 77010582). Individual nuclei were marked by creating a binary image, using the “Threshold” function, over the DAPI stain of the nuclei. Each nucleus was designated as a Region of Interest (ROI) by converting the binary image to an ROI. An additional polygonal ROI was manually created over a non-nuclear region of background stain and then that level of background was subtracted from the entire image. For each channel, average intensity of each nucleus was taken as the intensity measurements from individual ROIs. These intensity values of individual nuclei were then averaged to get the average intensity per embryo. Embryos with 2-3 cells were categorized as being at the 2-cell stage in development. The 4-cell stage encompassed embryos with 4-5 cells. Embryos with 6-10 cells were classified as being at the 8-cell stage in development, and the 16-cell stage encompassed embryos with 14-19 cells. To preserve IF intensities, the images of embryos were not deconvolved. Intensity data for individual nuclei is presented in Figure 2- source data 1.

The Threshold function of the software cannot always distinguish between two nuclei that are overlapping. Similarly, if a single nucleus is an odd shape, it may get counted as multiple nuclei by the software. Some embryos were therefore had different numbers of nuclei measured than how the number of cells in the embryo. If the number of cells in an embryo differs from the number of nuclei listed, the actual number of cells is indicated in parenthesis next to the embryo label in Figure 2- source data 1.

## RNA-Seq Sample Preparation

mRNA was isolated from whole embryos using the Dynabeads mRNA DIRECT Kit (Thermo Fisher, # 610.11) according to the manufacturer’s instructions. E3.5 embryos of similar sizes of all genotypes were used for RNA-Seq. *Eed*<sup>fl/-</sup> and *Eed*<sup>-/-</sup> embryos were genotyped by *Eed* RT-PCR and all embryo genotypes were confirmed by quantifying the relative expression of *Eed* exon 7 to the sample’s number of mapped reads (Figure 3- figure supplement 1 and Figure 4- figure supplement 1). Samples were submitted to the University of Michigan DNA Sequencing Core for Poly-A RNA purification and, separately, strand-specific library preparation using the Takara SMARTer Seq V4 stranded low input kit (Takara, #634889). All libraries were sequenced on the Illumina HiSeq2000 or HiSeq4000 platforms to generate 50 bp paired-end reads.

## Mapping of RNA-Seq Data

Quality control analysis of the RNA-Seq data was conducted using FastQC. SNP data from whole-genome sequencing of the 129/S1 (*M. musculus*) and JF1/Ms (*M. molossinus*) mouse strains were substituted into the mm9 mouse reference genome build (C57BL/6 J) using VCFtools to generate *in silico* 129/S1 and JF1/Ms reference genomes (Maclary et al., 2017). Sequencing reads were separately mapped to each of the two *in silico* genomes using STAR (Dobin et al., 2013), allowing 0 mismatches in mapped reads to ensure allele-specific mapping of SNP-containing reads to only one strain-specific genome. STAR was selected for read mapping, in part due to the improved ability to handle structural variability and indels, with the goal of reducing mapping bias to the genome most similar to the reference genome. STAR is a

spliced aligner capable of detecting structural variations and is able to handle small insertions and deletions during read mapping. STAR additionally permits soft-clipping of reads during mapping, trimming the ends of long reads that cannot be perfectly mapped. This function would permit clipping of reads that end near indels, thus preserving mappability at SNPs near indels.

Prior work showed that the variability due to mapping bias between the 129/S1 and JF1/Ms genomes is minimal (Maclary et al., 2017). Although small biases may affect allelic mapping at a subset of SNP sites within a gene, the effect is mitigated since most genes contain multiple SNPs (Figure 3- figure supplement 1).

## Allele-specific Analysis of RNA-Seq Data

For allelic expression analysis, only RNA-Seq reads overlapping known SNP sites that differ between the 129/S1 and JF1/Ms genomes were retained. All multi-mapping reads were excluded from the allele-specific analysis. For each SNP site, reads mapping to the 129/S1 and JF1/Ms X chromosomes were counted and the proportion of reads from each X chromosome identified. Allelic expression was calculated individually for each SNP site; for genes containing multiple SNPs, the paternal-X percentage for all SNPs was averaged to calculate gene-level allelic expression. All SNP sites with at least 10 SNP-overlapping reads were retained. Genes containing at least one SNP site with at least 10 SNP-overlapping reads were retained for further analysis and are referred to in the text as informative. In X-linked genes, the SNP frequency is ~1 SNP/250bp in transcribed RNAs (Keane et al., 2011; Maclary et al., 2017; Takada et al., 2013; Yalcin et al., 2011).

## RNA-Seq Expression Analysis

To calculate expression from the maternal vs. paternal X-chromosomes, all reads were first merged into a single alignment file and the number of reads per RefSeq annotated gene was counted using HTSeq. To calculate the percentage of expression arising from the paternal X-chromosome, the total read counts from HTSeq were normalized by number of mapped reads. Then, the normalized number of mapped reads for each gene was multiplied by the proportion of SNP-containing reads mapping to the paternal X-chromosome. This analysis was done in R using the following formula:

$$\left\{ \text{total reads} \times \left( \frac{\text{paternal reads}}{\text{maternal reads} + \text{paternal reads}} \right) \right\}$$

## Analysis of Human and Mouse Oocyte RNA-Seq Data

For analysis of publicly available oocyte RNA-Seq data, raw Fastq files were obtained from the NCBI Sequence Read Archive. Quality control analysis was conducted using FastQC. Reads were aligned to the mm9 (mouse) or hg19 (human) reference genome using STAR (Dobin et al., 2013) and counted using FeatureCounts (Liao, Smyth, & Shi, 2014). BioProject and Run numbers for samples analyzed are listed here.

Human oocyte RNA-Seq	
BioProject ID	Run Number
PRJNA146903	SRR351336

Mouse oocyte RNA-Seq	
BioProject ID	Run Number
PRJDB21	DRR001701

PRJNA146903	SRR351337	PRJDB21	DRR001702
PRJEB8994	ERR841204	PRJNA154207	SRR385627

## Statistical Analysis & Plots

Welch's two-sample T-tests were used to test for significant differences between the means of Pyrosequencing and RNA-Seq allelic expression data. This test was chosen due to the unequal variance and sample sizes between different genotype groups. In the RNA-Seq allelic expression significance tests, the average percent paternal expression of all informative X-linked genes was calculated for each sample. The total paternal expression value for each genotype group was calculated by calculating the mean of the informative percent paternal values for all samples in that genotype group. A two-tailed Student's T-test was used to determine the significance of RNA FISH and IF data. All barplots and heatmaps were made using the ggplot and Pheatmap R packages, respectively. Dotplots were made using Python's Seaborn package. Only genes that were informative in all samples were included in the heatmaps.

## Data Availability

RNA-Seq data generated for this study have been submitted to the NCBI Gene Expression Omnibus (GEO; <http://www.ncbi.nlm.nih.gov/geo/>) under accession number GSE123173.

## References

- Barlow, D. P. (2011). Genomic imprinting: a mammalian epigenetic discovery model. *Annu Rev Genet*, 45, 379-403. doi:10.1146/annurev-genet-110410-132459
- Borensztein, M., Syx, L., Ancelin, K., Diabangouaya, P., Picard, C., Liu, T., . . . Heard, E. (2017). Xist-dependent imprinted X inactivation and the early developmental consequences of its failure. *Nat Struct Mol Biol*, 24(3), 226-233. doi:10.1038/nsmb.3365
- Cao, R., Wang, L., Wang, H., Xia, L., Erdjument-Bromage, H., Tempst, P., . . . Zhang, Y. (2002). Role of histone H3 lysine 27 methylation in Polycomb-group silencing. *Science*, 298(5595), 1039-1043.
- Cloutier, M., Harris, C., Gayen, S., Maclary, E., & Kalantry, S. (2018). Experimental Analysis of Imprinted Mouse X-Chromosome Inactivation. *Methods Mol Biol*, 1861, 177-203. doi:10.1007/978-1-4939-8766-5\_14
- Czermin, B., Melfi, R., McCabe, D., Seitz, V., Imhof, A., & Pirrotta, V. (2002). Drosophila enhancer of Zeste/ESC complexes have a histone H3 methyltransferase activity that marks chromosomal Polycomb sites. *Cell*, 111(2), 185-196.
- de la Cruz, C. C., Fang, J., Plath, K., Worringer, K. A., Nusinow, D. A., Zhang, Y., & Panning, B. (2005). Developmental regulation of Suz 12 localization. *Chromosoma*, 114(3), 183-192.
- Dobin, A., Davis, C. A., Schlesinger, F., Drenkow, J., Zaleski, C., Jha, S., . . . Gingeras, T. R. (2013). STAR: ultrafast universal RNA-seq aligner. *Bioinformatics*, 29(1), 15-21. doi:10.1093/bioinformatics/bts635
- Faust, C., Schumacher, A., Holdener, B., & Magnuson, T. (1995). The eed mutation disrupts anterior mesoderm production in mice. *Development*, 121(2), 273-285.
- Ferguson-Smith, A. C., & Bourc'his, D. (2018). The discovery and importance of genomic imprinting. *Elife*, 7. doi:10.7554/eLife.42368
- Gayen, S., Maclary, E., Buttigieg, E., Hinten, M., & Kalantry, S. (2015). A Primary Role for the Tsix lncRNA in Maintaining Random X-Chromosome Inactivation. *Cell Rep*, 11(8), 1251-1265. doi:10.1016/j.celrep.2015.04.039
- Hadjantonakis, A. K., Gertsenstein, M., Ikawa, M., Okabe, M., & Nagy, A. (1998). Non-invasive sexing of preimplantation stage mammalian embryos. *Nat Genet*, 19(3), 220-222.
- Harper, M. I., Fosten, M., & Monk, M. (1982). Preferential paternal X inactivation in extraembryonic tissues of early mouse embryos. *J Embryol Exp Morphol*, 67, 127-135.
- Hinten, M., Maclary, E., Gayen, S., Harris, C., & Kalantry, S. (2016). Visualizing Long Noncoding RNAs on Chromatin. *Methods Mol Biol*, 1402, 147-164. doi:10.1007/978-1-4939-3378-5\_12
- Huynh, K. D., & Lee, J. T. (2003). Inheritance of a pre-inactivated paternal X chromosome in early mouse embryos. *Nature*, 426(6968), 857-862.

774 Inoue, A., Chen, Z., Yin, Q., & Zhang, Y. (2018). Maternal Eed knockout causes loss of  
775 H3K27me3 imprinting and random X inactivation in the extraembryonic cells. *Genes*  
776 *Dev*. doi:10.1101/gad.318675.118

777 Inoue, A., Jiang, L., Lu, F., & Zhang, Y. (2017). Genomic imprinting of Xist by maternal  
778 H3K27me3. *Genes Dev*, 31(19), 1927-1932. doi:10.1101/gad.304113.117

779 Kalantry, S. (2011). Recent advances in X-chromosome inactivation. *J Cell Physiol*, 226(7),  
780 1714-1718. doi:10.1002/jcp.22673

781 Kalantry, S., & Magnuson, T. (2006). The Polycomb group protein EED is dispensable for the  
782 initiation of random X-chromosome inactivation. *PLoS Genet*, 2(5), e66.  
783 doi:10.1371/journal.pgen.0020066

784 Kalantry, S., Mills, K. C., Yee, D., Otte, A. P., Panning, B., & Magnuson, T. (2006). The  
785 Polycomb group protein Eed protects the inactive X-chromosome from differentiation-  
786 induced reactivation. *Nat Cell Biol*, 8(2), 195-202. doi:ncb1351 [pii]  
787 10.1038/ncb1351

788 Kalantry, S., Purushothaman, S., Bowen, R. B., Starmer, J., & Magnuson, T. (2009). Evidence  
789 of Xist RNA-independent initiation of mouse imprinted X-chromosome inactivation.  
790 *Nature*, 460, 647-651. doi:nature08161 [pii]  
791 10.1038/nature08161

792 Kay, G. F., Barton, S. C., Surani, M. A., & Rastan, S. (1994). Imprinting and X chromosome  
793 counting mechanisms determine Xist expression in early mouse development. *Cell*,  
794 77(5), 639-650.

795 Keane, T. M., Goodstadt, L., Danecek, P., White, M. A., Wong, K., Yalcin, B., . . . Adams, D. J.  
796 (2011). Mouse genomic variation and its effect on phenotypes and gene regulation.  
797 *Nature*, 477(7364), 289-294. doi:10.1038/nature10413

798 Kobayashi, H., Sakurai, T., Imai, M., Takahashi, N., Fukuda, A., Yayoi, O., . . . Kono, T. (2012).  
799 Contribution of intragenic DNA methylation in mouse gametic DNA methylomes to  
800 establish oocyte-specific heritable marks. *PLoS Genet*, 8(1), e1002440.  
801 doi:10.1371/journal.pgen.1002440

802 Kohlmaier, A., Savarese, F., Lachner, M., Martens, J., Jenuwein, T., & Wutz, A. (2004). A  
803 chromosomal memory triggered by xist regulates histone methylation in x inactivation.  
804 *PLoS Biol*, 2(7), E171.

805 Kunath, T., Arnaud, D., Uy, G. D., Okamoto, I., Chureau, C., Yamanaka, Y., . . . Rossant, J.  
806 (2005). Imprinted X-inactivation in extra-embryonic endoderm cell lines from mouse  
807 blastocysts. *Development*, 132(7), 1649-1661. doi:132/7/1649 [pii]  
808 10.1242/dev.01715

809 Kuzmichev, A., Nishioka, K., Erdjument-Bromage, H., Tempst, P., & Reinberg, D. (2002).  
810 Histone methyltransferase activity associated with a human multiprotein complex  
811 containing the Enhancer of Zeste protein. *Genes Dev*, 16(22), 2893-2905.

812 Lee, J. T., & Bartolomei, M. S. (2013). X-inactivation, imprinting, and long noncoding RNAs in  
813 health and disease. *Cell*, 152(6), 1308-1323. doi:10.1016/j.cell.2013.02.016

814 Levesque, M. J., Ginart, P., Wei, Y., & Raj, A. (2013). Visualizing SNVs to quantify allele-  
815 specific expression in single cells. *Nat Methods*, 10(9), 865-867.  
816 doi:10.1038/nmeth.2589

817 Lewandoski, M., Wassarman, K. M., & Martin, G. R. (1997). Zp3-cre, a transgenic mouse line  
818 for the activation or inactivation of loxP-flanked target genes specifically in the female  
819 germ line. *Curr Biol*, 7(2), 148-151. doi:S0960-9822(06)00059-5 [pii]

820 Liao, Y., Smyth, G. K., & Shi, W. (2014). featureCounts: an efficient general purpose program  
821 for assigning sequence reads to genomic features. *Bioinformatics*, 30(7), 923-930.  
822 doi:10.1093/bioinformatics/btt656

823 Lyon, M. F. (1961). Gene action in the X-chromosome of the mouse (*Mus musculus* L.). *Nature*,  
824 190, 372-373.

825 Macfarlan, T. S., Gifford, W. D., Driscoll, S., Lettieri, K., Rowe, H. M., Bonanomi, D., . . . Pfaff, S.  
826 L. (2012). Embryonic stem cell potency fluctuates with endogenous retrovirus activity.  
827 *Nature*, 487(7405), 57-63. doi:10.1038/nature11244

828 Maclary, E., Buttigieg, E., Hinten, M., Gayen, S., Harris, C., Sarkar, M. K., . . . Kalantry, S.  
829 (2014). Differentiation-dependent requirement of Tsix long non-coding RNA in imprinted  
830 X-chromosome inactivation. *Nat Commun*, 5, 4209. doi:10.1038/ncomms5209

831 Maclary, E., Hinten, M., Harris, C., Sethuraman, S., Gayen, S., & Kalantry, S. (2017). PRC2  
832 represses transcribed genes on the imprinted inactive X chromosome in mice. *Genome*  
833 *Biol*, 18(1), 82. doi:10.1186/s13059-017-1211-5

834 Mak, W., Nesterova, T. B., de Napoles, M., Appanah, R., Yamanaka, S., Otte, A. P., &  
835 Brockdorff, N. (2004). Reactivation of the paternal X chromosome in early mouse  
836 embryos. *Science*, 303(5658), 666-669.

837 Margueron, R., & Reinberg, D. (2010). The Polycomb complex PRC2 and its mark in life.  
838 *Nature*, 469(7330), 343-349. doi:nature09784 [pii]

839 10.1038/nature09784

840 Matsui, J., Goto, Y., & Takagi, N. (2001). Control of Xist expression for imprinted and random X  
841 chromosome inactivation in mice. *Hum Mol Genet*, 10(13), 1393-1401.

842 Monk, M., & Kathuria, H. (1977). Dosage compensation for an X-linked gene in pre-implantation  
843 mouse embryos. *Nature*, 270(5638), 599-601.

844 Montgomery, N. D., Yee, D., Chen, A., Kalantry, S., Chamberlain, S. J., Otte, A. P., &  
845 Magnuson, T. (2005). The Murine Polycomb Group Protein Eed Is Required for Global  
846 Histone H3 Lysine-27 Methylation. *Curr Biol*, 15(10), 942-947.

847 Morey, C., & Avner, P. (2011). The demoiselle of X-inactivation: 50 years old and as trendy and  
848 mesmerising as ever. *PLoS Genet*, 7(7), e1002212. doi:10.1371/journal.pgen.1002212

849 PGENETICS-D-11-00997 [pii]

850 Muller, J., Hart, C. M., Francis, N. J., Vargas, M. L., Sengupta, A., Wild, B., . . . Simon, J. A.  
851 (2002). Histone methyltransferase activity of a Drosophila Polycomb group repressor  
852 complex. *Cell*, 111(2), 197-208.

853 Namekawa, S. H., Payer, B., Huynh, K. D., Jaenisch, R., & Lee, J. T. (2010). Two-step  
854 imprinted X inactivation: repeat versus genic silencing in the mouse. *Mol Cell Biol*,  
855 30(13), 3187-3205. doi:MCB.00227-10 [pii]

856 10.1128/MCB.00227-10

857 O'Gorman, S., Dagenais, N. A., Qian, M., & Marchuk, Y. (1997). Protamine-Cre recombinase  
858 transgenes efficiently recombine target sequences in the male germ line of mice, but not  
859 in embryonic stem cells. *Proc Natl Acad Sci U S A*, 94(26), 14602-14607.

860 Okamoto, I., Otte, A. P., Allis, C. D., Reinberg, D., & Heard, E. (2004). Epigenetic dynamics of  
861 imprinted X inactivation during early mouse development. *Science*, 303(5658), 644-649.  
862 doi:10.1126/science.1092727

863 1092727 [pii]

864 Okamoto, I., Patrat, C., Thepot, D., Peynot, N., Fauque, P., Daniel, N., . . . Heard, E. Eutherian  
865 mammals use diverse strategies to initiate X-chromosome inactivation during  
866 development. *Nature*, 472(7343), 370-374. doi:nature09872 [pii]

867 10.1038/nature09872

868 Okamoto, I., Tan, S., & Takagi, N. (2000). X-chromosome inactivation in XX androgenetic  
869 mouse embryos surviving implantation. *Development*, 127(19), 4137-4145.

870 Patrat, C., Okamoto, I., Diabangouaya, P., Vialon, V., Le Baccon, P., Chow, J., & Heard, E.  
871 (2009). Dynamic changes in paternal X-chromosome activity during imprinted X-  
872 chromosome inactivation in mice. *Proc Natl Acad Sci U S A*, 106(13), 5198-5203.  
873 doi:0810683106 [pii]

874 10.1073/pnas.0810683106

875 Penny, G. D., Kay, G. F., Sheardown, S. A., Rastan, S., & Brockdorff, N. (1996). Requirement  
876 for Xist in X chromosome inactivation [see comments]. *Nature*, 379(6561), 131-137.

877 Petropoulos, S., Edsgard, D., Reinius, B., Deng, Q., Panula, S. P., Codeluppi, S., . . . Lanner, F.  
878 (2016). Single-Cell RNA-Seq Reveals Lineage and X Chromosome Dynamics in Human  
879 Preimplantation Embryos. *Cell*, 167(1), 285. doi:10.1016/j.cell.2016.08.009

880 Plath, K., Fang, J., Mlynarczyk-Evans, S. K., Cao, R., Worringer, K. A., Wang, H., . . . Zhang, Y.  
881 (2003). Role of histone H3 lysine 27 methylation in X inactivation. *Science*, 300(5616),  
882 131-135.

883 Plath, K., Mlynarczyk-Evans, S., Nusinow, D. A., & Panning, B. (2002). Xist RNA and the  
884 mechanism of X chromosome inactivation. *Annu Rev Genet*, 36, 233-278.

885 Prokopuk, L., Stringer, J. M., White, C. R., Vossen, R., White, S. J., Cohen, A. S. A., . . .  
886 Western, P. S. (2018). Loss of maternal EED results in postnatal overgrowth. *Clin*  
887 *Epigenetics*, 10(1), 95. doi:10.1186/s13148-018-0526-8

888 Rastan, S., Kaufman, M. H., Handyside, A. H., & Lyon, M. F. (1980). X-chromosome inactivation  
889 in extra-embryonic membranes of diploid parthenogenetic mouse embryos  
890 demonstrated by differential staining. *Nature*, 288(5787), 172-173.

891 Reich, A., Klatsky, P., Carson, S., & Wessel, G. (2011). The transcriptome of a human polar  
892 body accurately reflects its sibling oocyte. *J Biol Chem*, 286(47), 40743-40749.  
893 doi:10.1074/jbc.M111.289868

894 Sarkar, M. K., Gayen, S., Kumar, S., Maclary, E., Buttigieg, E., Hinten, M., . . . Kalantriy, S.  
895 (2015). An Xist-activating antisense RNA required for X-chromosome inactivation. *Nat*  
896 *Commun*, 6, 8564. doi:10.1038/ncomms9564

897 Shin, J., Bossenz, M., Chung, Y., Ma, H., Byron, M., Taniguchi-Ishigaki, N., . . . Bach, I. (2010).  
898 Maternal Rnf12/RLIM is required for imprinted X-chromosome inactivation in mice.  
899 *Nature*, 467(7318), 977-981. doi:nature09457 [pii]  
900 10.1038/nature09457

901 Shumacher, A., Faust, C., & Magnuson, T. (1996). Positional cloning of a global regulator of  
902 anterior-posterior patterning in mice. *Nature*, 383(6597), 250-253.

903 Silva, J., Mak, W., Zvetkova, I., Appanah, R., Nesterova, T. B., Webster, Z., . . . Brockdorff, N.  
904 (2003). Establishment of histone h3 methylation on the inactive X chromosome requires  
905 transient recruitment of Eed-Enx1 polycomb group complexes. *Dev Cell*, 4(4), 481-495.

906 Takada, T., Ebata, T., Noguchi, H., Keane, T. M., Adams, D. J., Narita, T., . . . Shiroishi, T.  
907 (2013). The ancestor of extant Japanese fancy mice contributed to the mosaic genomes  
908 of classical inbred strains. *Genome Res*, 23(8), 1329-1338. doi:10.1101/gr.156497.113

909 Takagi, N., & Sasaki, M. (1975). Preferential inactivation of the paternally derived X  
910 chromosome in the extraembryonic membranes of the mouse. *Nature*, 256(5519), 640-  
911 642.

912 Tanaka, S., Kunath, T., Hadjantonakis, A. K., Nagy, A., & Rossant, J. (1998). Promotion of  
913 trophoblast stem cell proliferation by FGF4. *Science*, 282(5396), 2072-2075.

914 van Otterdijk, S. D., & Michels, K. B. (2016). Transgenerational epigenetic inheritance in  
915 mammals: how good is the evidence? *FASEB J*, 30(7), 2457-2465.  
916 doi:10.1096/fj.201500083

917 Wang, F., Shin, J., Shea, J. M., Yu, J., Boskovic, A., Byron, M., . . . Bach, I. (2016). Regulation  
918 of X-linked gene expression during early mouse development by Rlim. *Elife*, 5.  
919 doi:10.7554/eLife.19127

920 Wang, J., Mager, J., Chen, Y., Schneider, E., Cross, J. C., Nagy, A., & Magnuson, T. (2001).  
921 Imprinted X inactivation maintained by a mouse Polycomb group gene. *Nat Genet*,  
922 28(4), 371-375.



923 West, J. D., Frels, W. I., Chapman, V. M., & Papaioannou, V. E. (1977). Preferential expression  
924 of the maternally derived X chromosome in the mouse yolk sac. *Cell*, 12(4), 873-882.

925 Yalcin, B., Wong, K., Agam, A., Goodson, M., Keane, T. M., Gan, X., . . . Flint, J. (2011).  
926 Sequence-based characterization of structural variation in the mouse genome. *Nature*,  
927 477(7364), 326-329. doi:10.1038/nature10432

928 Zheng, H., Huang, B., Zhang, B., Xiang, Y., Du, Z., Xu, Q., . . . Xie, W. (2016). Resetting  
929 Epigenetic Memory by Reprogramming of Histone Modifications in Mammals. *Mol Cell*,  
930 63(6), 1066-1079. doi:10.1016/j.molcel.2016.08.032

931

932

933

934

935

936

937

938

939

940

941

942

943

944

**Figure 1. Coincident accumulation of EED and H3K27me3 on the inactive X-chromosome in blastocyst-stage WT, *Eed*<sup>+/-</sup> and *Eed*<sup>-/-</sup> mouse embryos. See also Figure 1– figure supplement 1.**

**(A,B)** RNA FISH detection of Xist RNA (white) and immunofluorescence (IF) detection of EED (red) and H3K27me3 (green) in representative female and male wild-type (WT) **(A)** or female *Eed*<sup>+/-</sup> and *Eed*<sup>-/-</sup> **(B)** E3.0 – E3.5 blastocyst embryos. Nuclei are stained blue with DAPI. Scale bars, 20 µm. Embryos ranged in size from 23 to 57 nuclei. Bar plots, percentage of nuclei with coincident accumulation of Xist RNA and EED and/or H3K27me3 enrichment in individual embryos.

**(C)** Genotype and sex distribution of *Eed*<sup>+/-</sup> and *Eed*<sup>-/-</sup> mouse blastocyst embryos from the cross in **B**. The difference between the frequency of *Eed*<sup>+/-</sup> vs *Eed*<sup>-/-</sup> male and female embryos is not significant. (p > 0.05, Two-tailed Student's T-test).

**Figure 1– figure supplement 1. Generation of *Eed*<sup>-/-</sup> embryos.**

**(A)** Schematic depicting the deletion of floxed *Eed* exon 7 by CRE recombinase.

**(B)** Breeding data showing the efficiency of *Prm-Cre* deletion of the *Eed*<sup>fl</sup> allele.

**Figure 2. Assessment of maternal and zygotic EED expression in early preimplantation embryos. See also Figure 2– figure supplement 1, and Figure 2- source data 1.**

**(A,B)** Immunofluorescent (IF) detection of EED (red) and H3K27me3 mark (green) in 2- and 16-cell *Eed<sup>fl/fl</sup>*, *Eed<sup>fl/-</sup>* / *Eed<sup>+/-</sup>*, *Eed<sup>m/-</sup>*, and *Eed<sup>mz/-</sup>* embryos. Nuclei are stained blue by DAPI.

**(C)** Dot plots of EED and H3K27me3 IF signals in the five genotypes (*Eed<sup>fl/fl</sup>*, *Eed<sup>fl/-</sup>*, *Eed<sup>+/-</sup>*, *Eed<sup>m/-</sup>*, *Eed<sup>mz/-</sup>*) at the ~2-cell, ~4-cell, ~8-cell, and ~16-cell stage. Each dot represents an individual embryo. The gray line indicates mean signal intensity. Pairwise statistical comparisons between all genotypes are included in **Supplementary File 1**.

**(D)** Significance testing of differences in EED intensity in ~2-cell embryos and ~16-cell embryos plotted in **C** (Two-tailed Student's T-test).

**(E)** Mean EED intensity from data in **C** plotted across early embryogenesis.

**(F)** Model of change in maternal, zygotic, and total EED expression levels during early embryonic development.

**Figure 2 – figure supplement 1. Analysis of EED and H3K27me2 intensity in *Eed* mutants.**

**(A)** Schematic depicting the deletion of *Eed* exon 7 by *Zp3-Cre* used to generate embryos maternally null for *Eed*.

**(B)** Representative images of *Eed<sup>fl/fl</sup>*, *Eed<sup>fl/-</sup>*, *Eed<sup>+/-</sup>*, *Eed<sup>m/-</sup>*, and *Eed<sup>mz/-</sup>* 4- and 8-cell embryos stained by IF for EED and H3K27me3. Nuclei are indicated by blue DAPI stain, EED stain is indicated in red, and H3K27me3 stain is indicated in green.

**Figure 2- source data 2. Raw IF intensity data of individual nuclei.**

Intensity values for individual nuclei of each embryo plotted in Figure 2C. All nuclei from individual embryos were averaged to calculate the mean intensity of each embryo.

**Figure 3. Lack of defective X-inactivation initiation in *Eed*<sup>fl/-</sup> blastocysts. See also Figure 3– figure supplement 1.**

**(A)** Allele-specific X-linked gene expression heat map of female *Eed*<sup>fl/fl</sup>, *Eed*<sup>fl/-</sup>, and *Eed*<sup>+/-</sup> blastocysts. Four embryos each of *Eed*<sup>fl/fl</sup>, *Eed*<sup>fl/-</sup>, and *Eed*<sup>+/-</sup> genotypes were sequenced individually and only genes with informative allelic expression in all samples are plotted (see Materials and Methods). Genes are ordered on the basis of allelic expression in *Eed*<sup>fl/fl</sup> embryos.

**(B)** Average allelic expression of the RNA-Seq data shown in **A**. The mean allelic expression of X-linked genes lacks significant difference between each combination of the three genotypes ( $p > 0.05$ , Welch's two-sample T-test). Pairwise statistical comparisons between all genotypes are included in **Supplementary File 3**.

**(C)** Pyrosequencing-based quantification of allelic expression of X-linked genes *Xist*, *Rnf12*, *Atrx* and *Pgk1* in *Eed*<sup>fl/fl</sup>, *Eed*<sup>fl/-</sup>, and *Eed*<sup>+/-</sup> blastocysts. Error bars represent the standard deviation of data from 3-6 independent blastocyst embryos. The mean allelic expression of all four genes is not significantly different between each combination of the three genotypes ( $p > 0.05$ , Welch's two-sample T-test). Pairwise statistical comparisons for all genes and between all genotypes are included in **Supplementary File 4**.

**(D)** RNA FISH detection of *Xist* RNA (green), *Rnf12* RNA (red), and IF detection of H3K27me3 (white) in representative *Eed*<sup>fl/fl</sup> or *Eed*<sup>+/-</sup> female blastocysts. Nuclei are stained blue with DAPI. Scale bars, 20  $\mu$ m. Individual nuclei displaying representative categories of stains are shown to the right of each embryo. Embryos ranged in size from 39 to 100 nuclei.

**(E)** Bar plot of percentage of nuclei with coincident accumulation of *Xist* RNA and H3K27me3 in individual *Eed*<sup>fl/fl</sup> and *Eed*<sup>+/-</sup> embryos. Each bar is an individual embryo. Embryo numbers under the bars correspond to the same embryos plotted in **F**.

**(F)** Bar plots of percentage of nuclei with or without *Xist* RNA-coating and *Rnf12* RNA expression in the embryos stained in **D** and plotted in **E**. The numbers under the bars correspond to the same embryos plotted in **E**.

**Figure 3– figure supplement 1. X-linked gene expression analysis in *Eed*<sup>+/−</sup> embryos.**

**(A)** Validation of genotypes of E3.5 *Eed*<sup>fl/fl</sup>, *Eed*<sup>fl/−</sup>, and *Eed*<sup>+/−</sup> female blastocyst embryos. *Eed* exon 7 RNA-Seq reads are normalized to total mapped RNA-Seq reads.

**(B)** Table describing the RNA-Seq genotypes, number of sequenced embryos, average % maternal X-linked gene expression, average number of SNPs per X-linked gene, and the SNP overlapping read coverage threshold. A comprehensive list of expression levels of all informative genes is included in **Supplementary File 2**.

**(C)** Pyrosequencing-based quantification of allelic expression of X-linked genes *Xist*, *Rnf12*, *Atrx*, and *Pgk1* in individual *Eed*<sup>fl/fl</sup>, *Eed*<sup>fl/−</sup>, and *Eed*<sup>+/−</sup> female blastocysts. Error bars, standard deviation of data from 3-6 independent embryos. The mean allelic expression of all four genes lacks significant difference between each combination of the three genotypes ( $p > 0.05$ , Welch's two-sample T-test). Pairwise statistical comparisons for all genes and between all genotypes are included in **Supplementary File 4**.

**(D)** RNA FISH detection of *Xist* RNA (green), *Rnf12* RNA (red), and IF detection of H3K27me3 (white) in representative *Eed*<sup>fl/fl</sup> and *Eed*<sup>fl/−</sup> or *Eed*<sup>+/−</sup> male blastocysts. Nuclei are stained blue with DAPI. Scale bars, 20  $\mu$ m. Right of each embryo, individual nuclei displaying representative categories of stains. Embryos ranged in size from 56 to 65 nuclei. Bar plot, percentage of nuclei with or without *Xist* RNA-coating and *Rnf12* RNA expression.

**Figure 4. Defective imprinted X-inactivation initiation in blastocysts lacking maternal EED. See also Figure 4– figure supplement 1.**

**(A)** RNA FISH detection of Xist RNA (green) and IF stain for H3K27me3 (white) in representative *Eed<sup>m-/-</sup>* and *Eed<sup>mz-/-</sup>* female blastocysts. Nuclei are stained blue with DAPI. Scale bars, 20  $\mu$ m. *Eed<sup>fl/fl</sup>* blastocyst from Figure 3D shown for comparison. Right, individual representative nuclei. Mutant embryos ranged in size from 46 to 80 nuclei. Bar plot shows percentage of nuclei in each embryo analyzed that display H3K27me3 enrichment on the Xist RNA-coated X-chromosome.

**(B)** Maternal:paternal X-linked gene expression heat map of female *Eed<sup>m-/-</sup>* and *Eed<sup>mz-/-</sup>* blastocysts. Five *Eed<sup>m-/-</sup>* and three *Eed<sup>mz-/-</sup>* embryos were sequenced individually and only genes with informative allelic expression in all samples are plotted (see Materials and Methods). *Eed<sup>fl/fl</sup>*, *Eed<sup>fl/-</sup>*, and *Eed<sup>-/-</sup>* data from Figure 3A shown for comparison. Genes are ordered on the basis of allelic expression in *Eed<sup>fl/fl</sup>* embryos.

**(C)** Average maternal:paternal X-linked gene expression ratio from the RNA-Seq data shown in B. *Eed<sup>fl/fl</sup>*, *Eed<sup>fl/-</sup>*, and *Eed<sup>-/-</sup>* data from Figure 3B shown for comparison. The mean allelic expression of X-linked genes is significantly different between *Eed<sup>m-/-</sup>* and *Eed<sup>fl/fl</sup>*, and *Eed<sup>mz-/-</sup>* and *Eed<sup>fl/fl</sup>* blastocysts. ( $p < 0.05$ , Welch's two-sample T-test). Pairwise statistical comparisons between all genotype groups are included in **Supplementary File 3**.

**(D)** Average normalized maternal and paternal X-linked gene expression in blastocysts. Maternal and paternal X-linked gene expression is significantly different between *Eed<sup>m-/-</sup>* and *Eed<sup>mz-/-</sup>* embryos compared to *Eed<sup>fl/fl</sup>* embryos (\*,  $p < 0.05$ , Two-tailed Student's T-test). Pairwise statistical comparisons between all genotypes are included in **Supplementary File 3**.

**(E)** Pyrosequencing-based quantification of allelic expression of X-linked genes in *Eed<sup>m-/-</sup>* and *Eed<sup>mz-/-</sup>* blastocysts. *Eed<sup>fl/fl</sup>* data from Figure 3C are shown for comparison. Error bars represent the standard deviation of data from 3-6 independent blastocyst embryos. The mean allelic expression of *Xist*, *Rnf12*, and *Atrx* is significantly different between *Eed<sup>-/-</sup>* and *Eed<sup>m-/-</sup>* embryos. The mean allelic expression of *Rnf12*, *Pgk1*, and *Atrx* is

significantly different between *Eed*<sup>+/−</sup> and *Eed*<sup>mz/−</sup> embryos ( $p < 0.05$ , Welch's two-sample T-test). Pairwise statistical comparisons for all genes and between all genotypes are included in **Supplementary File 4**.

**Figure 4— figure supplement 1. Generation and X-linked gene profiling of *Eed*<sup>m/−</sup> and *Eed*<sup>mz/−</sup> embryos.**

**(A)** Validation of genotypes of E3.5 female embryos. *Eed* exon 7 RNA-Seq reads are normalized to total mapped RNA-Seq reads.

**(B)** Table describing the RNA-Seq genotypes, number of sequenced embryos, average percentage maternal X-linked gene expression, average number of SNPs per X-linked gene, and the SNP overlapping read coverage threshold. A comprehensive list of expression levels of all informative genes is included in **Supplementary File 2**.

**(C)** Normalized maternal or paternal reads per X-linked gene in individual *Eed*<sup>fl/fl</sup>, *Eed*<sup>fl/−</sup>, *Eed*<sup>+/−</sup>, *Eed*<sup>m/−</sup>, and *Eed*<sup>mz/−</sup> female E3.5 blastocysts.

**(D)** Pyrosequencing-based quantification of allelic expression of X-linked genes *Xist*, *Rnf12*, *Atrx*, and *Pgk1* in individual *Eed*<sup>fl/fl</sup>, *Eed*<sup>m/−</sup>, and *Eed*<sup>mz/−</sup> female E3.5 blastocysts. Error bars, standard deviation of data from 3-6 independent embryos. The mean allelic expression for *Xist*, *Rnf12*, and *Atrx* is significantly different between *Eed*<sup>fl/fl</sup> and *Eed*<sup>m/−</sup> embryos ( $p < 0.05$ , Welch's two-sample T-test). The mean allelic expression for *Xist*, *Rnf12*, *Atrx*, and *Pgk1* is significantly different between *Eed*<sup>fl/fl</sup> and *Eed*<sup>mz/−</sup> embryos ( $p < 0.05$ , Welch's two-sample T-test). The mean allelic expression of *Pgk1* is significantly different between *Eed*<sup>m/−</sup> and *Eed*<sup>mz/−</sup> embryos ( $p < 0.05$ , Welch's two-sample T-test). Pairwise statistical comparisons for all genes and between all genotypes are included in **Supplementary File 4**.

**(E)** Allele-specific H3K27me3 ChIP-Seq at the *Xist* locus of wild-type MII oocyte, sperm, PN5 zygote, 8-cell embryo, and inner cell mass (ICM) (Zheng et al., 2016).

**Figure 5. RNA FISH analysis of X-inactivation in *Eed*<sup>m-/-</sup> and *Eed*<sup>mz-/-</sup> blastocysts.**

**(A,B)** RNA FISH detection of Xist RNA (green) and Rnf12 RNA (red) in representative *Eed*<sup>m-/-</sup> and *Eed*<sup>mz-/-</sup> female **(A)** and *Eed*<sup>mz-/-</sup> male **(B)** blastocysts. Nuclei are stained blue with DAPI. Scale bars, 20  $\mu$ m. Individual nuclei of representative categories of stain are shown to the right of each embryo. *Eed*<sup>fl/fl</sup> female data from Figure 3D shown for comparison. Mutant female embryos ranged in size from 46 to 80 nuclei. Fully developed mutant male embryos ranged in size from 53 to 110 nuclei. Delayed mutant male embryos ranged in size from 30-40 nuclei. Bar plot shows percentage of nuclei in each embryo with Xist RNA coats and/or Rnf12 RNA expression. Each bar represents an individual embryo and embryo numbers under the bars correspond to the same female embryos plotted in Figure 4A. \*, p<0.05; \*\*, p< 0.01, Two-tailed Student's T-test, between *Eed*<sup>m-/-</sup> and *Eed*<sup>fl/fl</sup>, or *Eed*<sup>mz-/-</sup> and *Eed*<sup>fl/fl</sup>.

**(C)** Data showing the number of *Eed*<sup>m-/-</sup> embryos which can live to term compared to *Eed*<sup>fl/fl</sup> embryos. WT, wild-type. Table shows *Eed*<sup>m-/-</sup> litters sired by *Mus musculus*-derived male or *Mus molossinus*-derived male. Male *Eed*<sup>m-/-</sup> offspring are underrepresented compared to females, p=.02, Two-tailed Student's T-test.



**Figure 6. Switching of imprinted to random X-inactivation in E3.5 embryos lacking maternal EED. See also Figure 6– figure supplement 1.**

**(A,B)** Allele-Specific Xist RNA FISH in *Eed*<sup>fl/+</sup> and *Eed*<sup>m-/-</sup> male and female E3.0-E3.5 blastocyst embryos. Xist RNA expressed from the maternal X-chromosome is indicated in red and from the paternal X-chromosome in white. Representative embryos are depicted. Nuclei are stained blue with DAPI. Scale bars, 20  $\mu$ m.

**Figure 6– figure supplement 1. Characterization of allele-specific Xist RNA FISH probe in cells and embryos.**

**(A)** Female Trophoblast stem (TS) cells (top panel) and extraembryonic endoderm (XEN) stem cells (bottom panel) stained with an allele-specific Xist RNA FISH probe. Both TS cells and XEN cells express *Xist* from and undergo imprinted X-inactivation of the paternal X-chromosome (Kunath et al., 2005; Tanaka, Kunath, Hadjantonakis, Nagy, & Rossant, 1998). The TS cells are derived from a cross of JF1 *Mus molossinus* dam with a 129/S1-derived *Mus musculus* sire. The XEN cells are generated from a cross of 129/S1 *Mus musculus* dam and JF1 *Mus molossinus*-derived sire. In the TS cells, the paternal-X is therefore *Mus musculus* derived while in the XEN cells the paternal-X is JF1 *Mus molossinus* derived. *Mus musculus*-specific Xist RNA FISH probe detects the complimentary Xist RNA in red and the *Mus molossinus*-specific Xist RNA FISH probe detects its complimentary Xist RNA in white.

**(B)** *Eed*<sup>fl/+</sup> female E3.5 embryos stained with the same allele-specific Xist RNA FISH probe as in **A**. Top panels, representative stained embryo derived from a cross of *Eed*<sup>fl/fl</sup> X<sup>JF1</sup>X<sup>JF1</sup> *Mus molossinus*-derived dam with a *Mus musculus* sire. Bottom panels, representative stained embryo from an *Eed*<sup>fl/fl</sup> *Mus musculus*-derived dam with a JF1 *Mus molossinus*-derived sire (this embryo is also shown in Figure 6A). Due to imprinted X-inactivation, both E3.5 embryos are expected to express Xist RNA from their paternal X-chromosome.

**Figure 7. Switching of imprinted to random X-inactivation in 3-16 cell embryos lacking maternal EED.**

**(A,B)** Allele-Specific Xist RNA FISH in *Eed<sup>fl/+</sup>* and *Eed<sup>m-/-</sup>* female and male 3-16 cell embryos. Xist RNA expressed from the maternal X-chromosome is indicated in red and from the paternal X-chromosome in white. Representative embryos are depicted. Nuclei are stained blue with DAPI. Scale bars, 20  $\mu$ m.

**Figure 8. Lack of PRC2 expression in human oocytes and a path to randomization of X-inactivation in early embryos.**

**(A)** Expression levels by RNA-Seq of core PRC2 components in human and mouse oocytes.

**(B)** Model of maternal PRC2 function during preimplantation mouse embryogenesis.

1223 **Supplementary File 1. Pairwise analysis of IF intensity data in Figure 2.**

1224 Statistical comparisons of EED and H3K27me3 IF intensities between all genotypes at each  
1225 embryonic stage analyzed in Figure 2 (Two-tailed Student's T-test).

1226

1227 **Supplementary File 2. Percentage of total X-linked gene expression from the paternal X-**  
1228 **chromosome by RNA-Seq.**

1229 Analysis of each informative X-linked gene ( $\geq 10$  reads/SNP).

1230

1231 **Supplementary File 3. Pairwise analysis of RNA-Seq data.**

1232 Statistical comparisons of percent allelic expression from the paternal X-chromosome and  
1233 normalized expression from the paternal- or maternal-X of all genotypes.

1234

1235 **Supplementary File 4. Pairwise analysis of Pyrosequencing data.**

1236 Statistical comparisons of Pyrosequencing data of *Xist*, *Rnf12*, *Atrx*, and *Pgk1* RNAs in embryos  
1237 of all genotypes.

1238

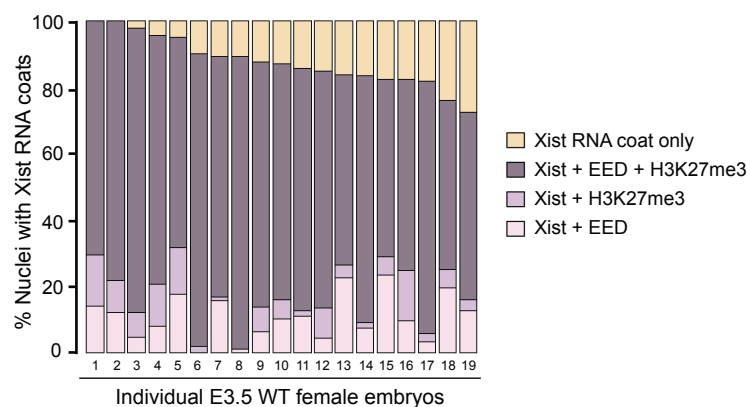
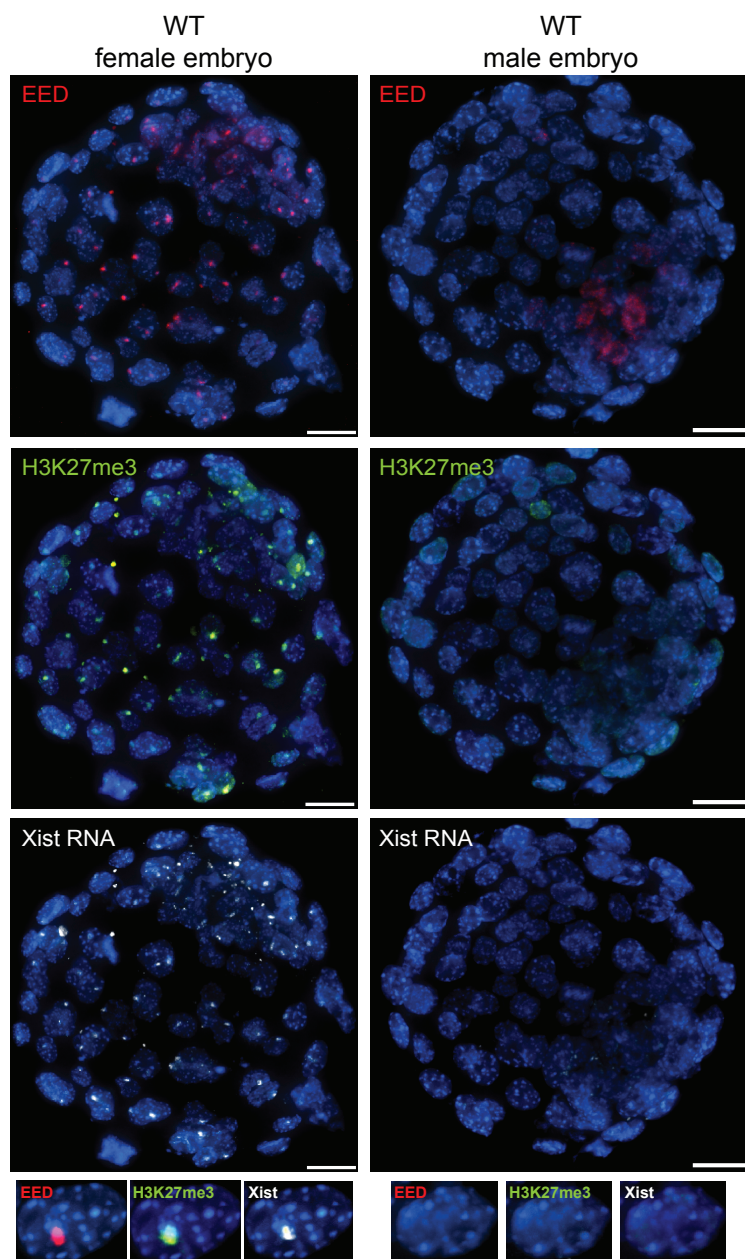
1239 **Supplementary File 5. Primer sequences and antibody information.**

1240 Primer sequences for Pyrosequencing, RT-PCR, genomic PCR, and allele-specific RNA FISH  
1241 probes; and, antibody information.

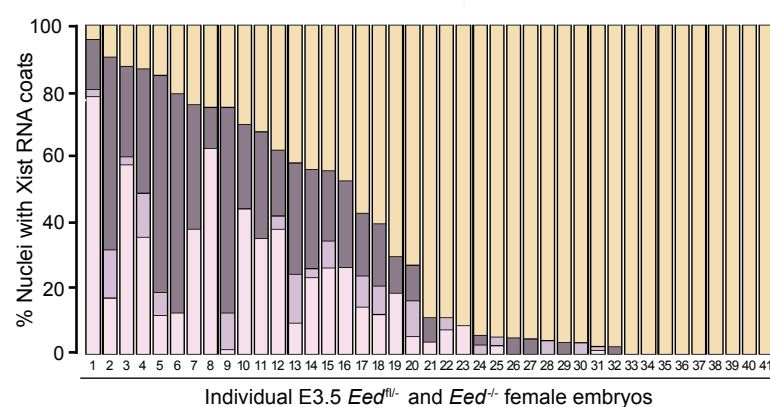
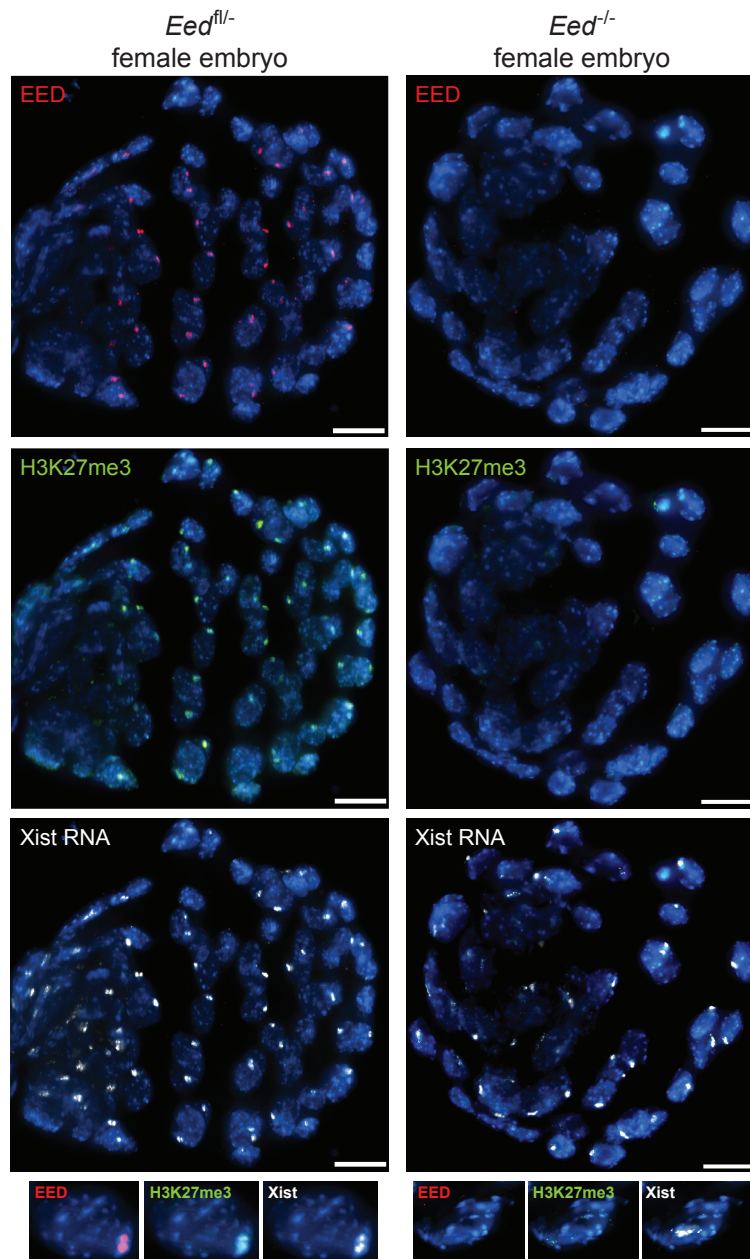
1242

1243

A



B

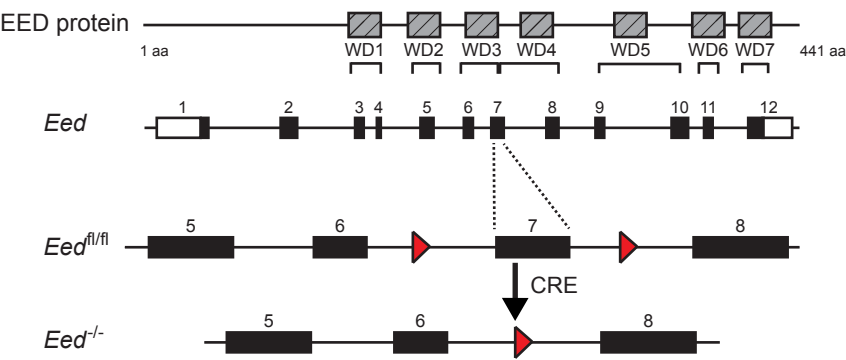


C

Distribution of E3.5 Embryos (12 litters)

Genotype	Females	Males
<i>Eed<sup>fl/-</sup></i>	16	12
<i>Eed<sup>-/-</sup></i>	9	15

A



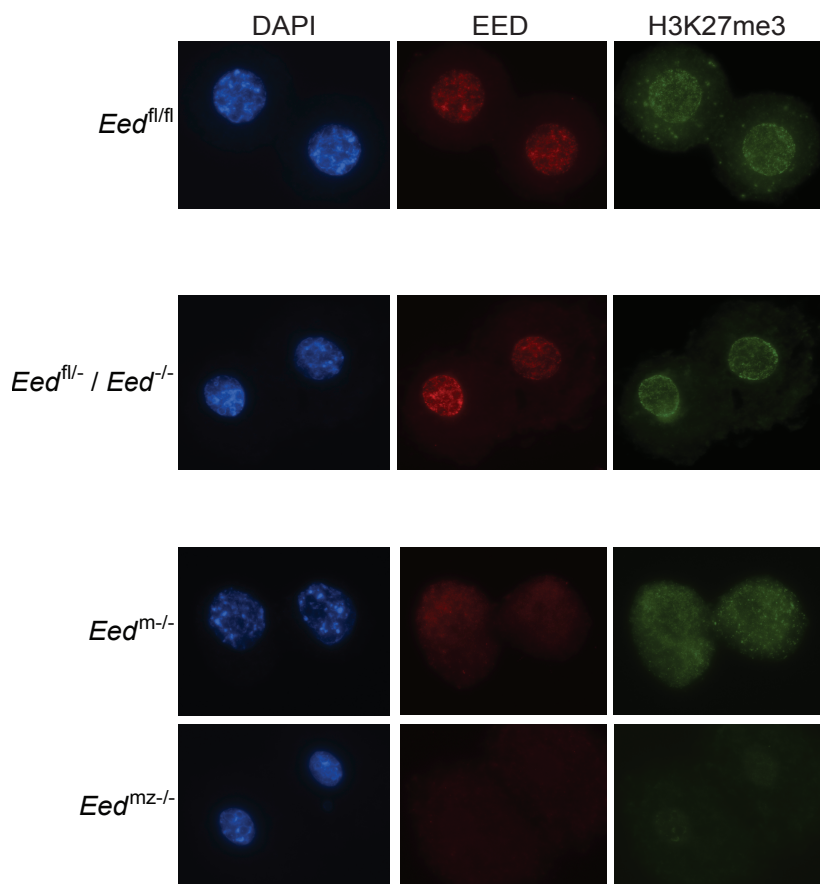
B

*Eed<sup>fl</sup>* deletion efficiency by *Prm-Cre*

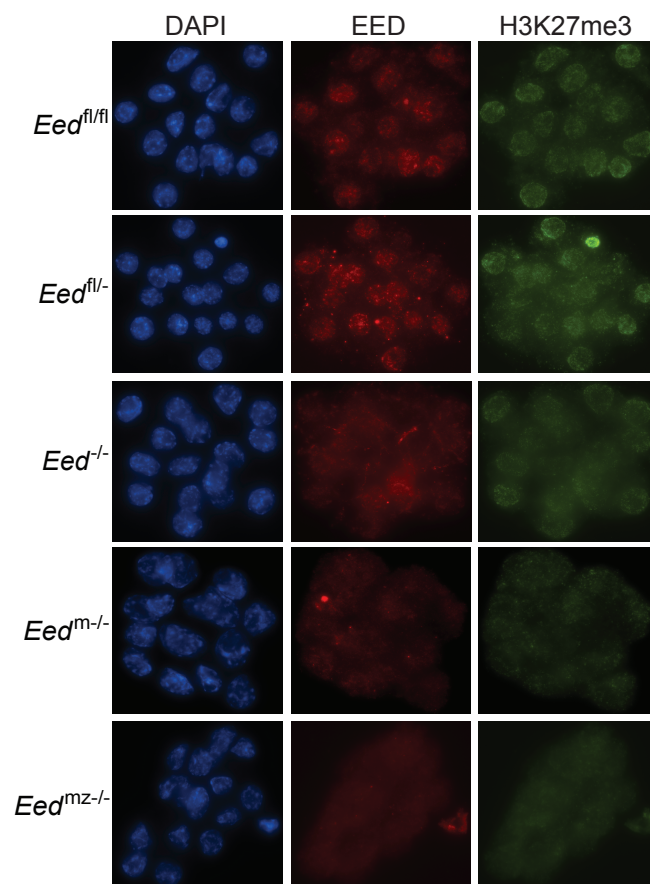
Dam	Sire	Number of litters	Number of pups	<i>Eed<sup>fl/fl</sup></i> pups	<i>Eed<sup>fl/-</sup></i> or <i>Eed<sup>+/-</sup></i> pups
<i>Eed<sup>fl/fl</sup></i>	<i>Eed<sup>fl/fl</sup>;Prm-Cre</i>	6	36	4 (11%)	32 (89%)
<i>Eed<sup>fl/fl</sup></i> or WT	<i>Eed<sup>fl/-</sup>;Prm-Cre</i>	17	88	8 (9%)	80 (91%)

**A**

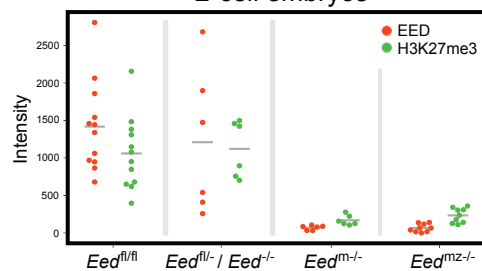
2-cell embryos

**B**

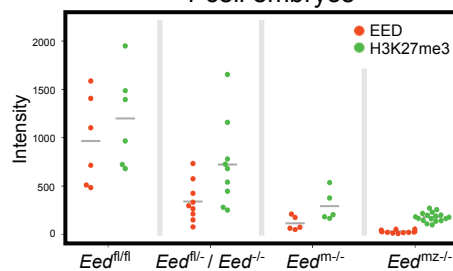
16-cell embryos

**C**

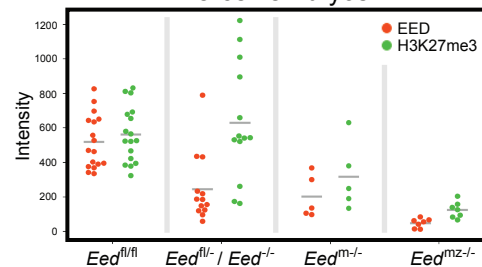
~2-cell embryos



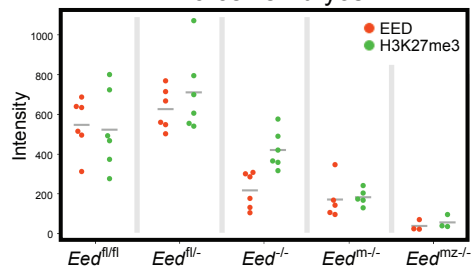
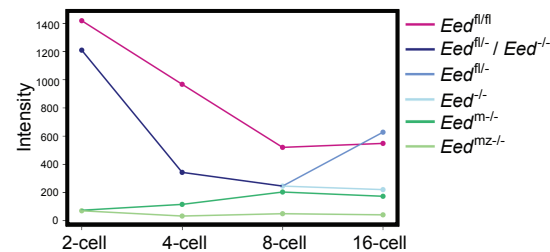
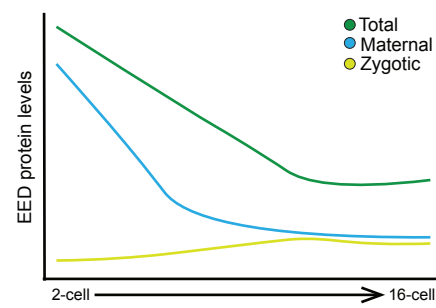
~4-cell embryos



~8-cell embryos



~16-cell embryos

**E****F****D**

p-values of ~2-cell embryo EED IF intensity

	<i>Eed<sup>fl/fl</sup></i>	<i>Eed<sup>fl/-</sup> / Eed<sup>-/-</sup></i>	<i>Eed<sup>m/-</sup></i>	<i>Eed<sup>mz/-</sup></i>
<i>Eed<sup>fl/fl</sup></i>				
<i>Eed<sup>fl/-</sup> / Eed<sup>-/-</sup></i>	0.58			
<i>Eed<sup>m/-</sup></i>	$5 \times 10^{-5}$	0.02		
<i>Eed<sup>mz/-</sup></i>	$2 \times 10^{-6}$	$3 \times 10^{-3}$	0.88	

p-values of ~16-cell embryo EED IF intensity

	<i>Eed<sup>fl/fl</sup></i>	<i>Eed<sup>fl/-</sup></i>	<i>Eed<sup>-/-</sup></i>	<i>Eed<sup>m/-</sup></i>	<i>Eed<sup>mz/-</sup></i>
<i>Eed<sup>fl/fl</sup></i>					
<i>Eed<sup>fl/-</sup></i>	0.29				
<i>Eed<sup>-/-</sup></i>	$6 \times 10^{-4}$	$3 \times 10^{-5}$			
<i>Eed<sup>m/-</sup></i>	$7 \times 10^{-4}$	$5 \times 10^{-5}$	0.44		
<i>Eed<sup>mz/-</sup></i>	$5 \times 10^{-4}$	$4 \times 10^{-5}$	0.01	0.08	



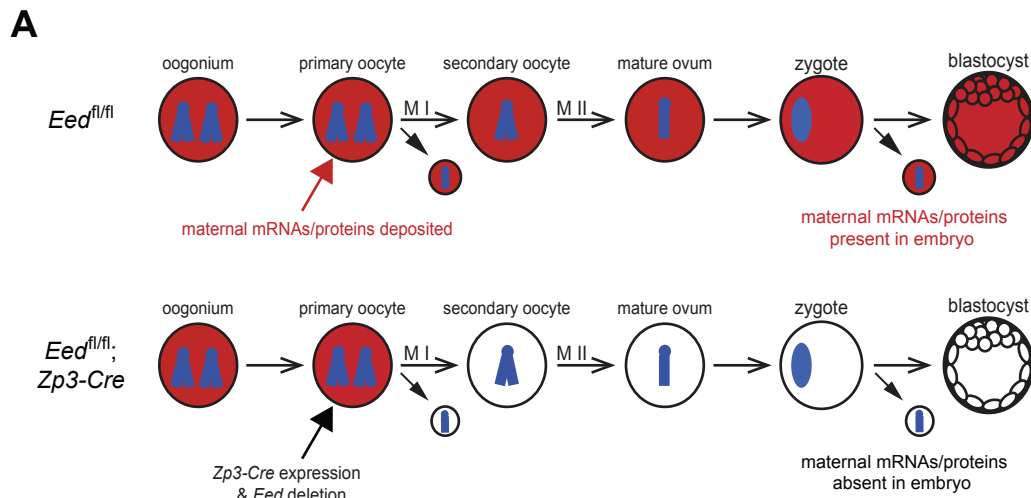
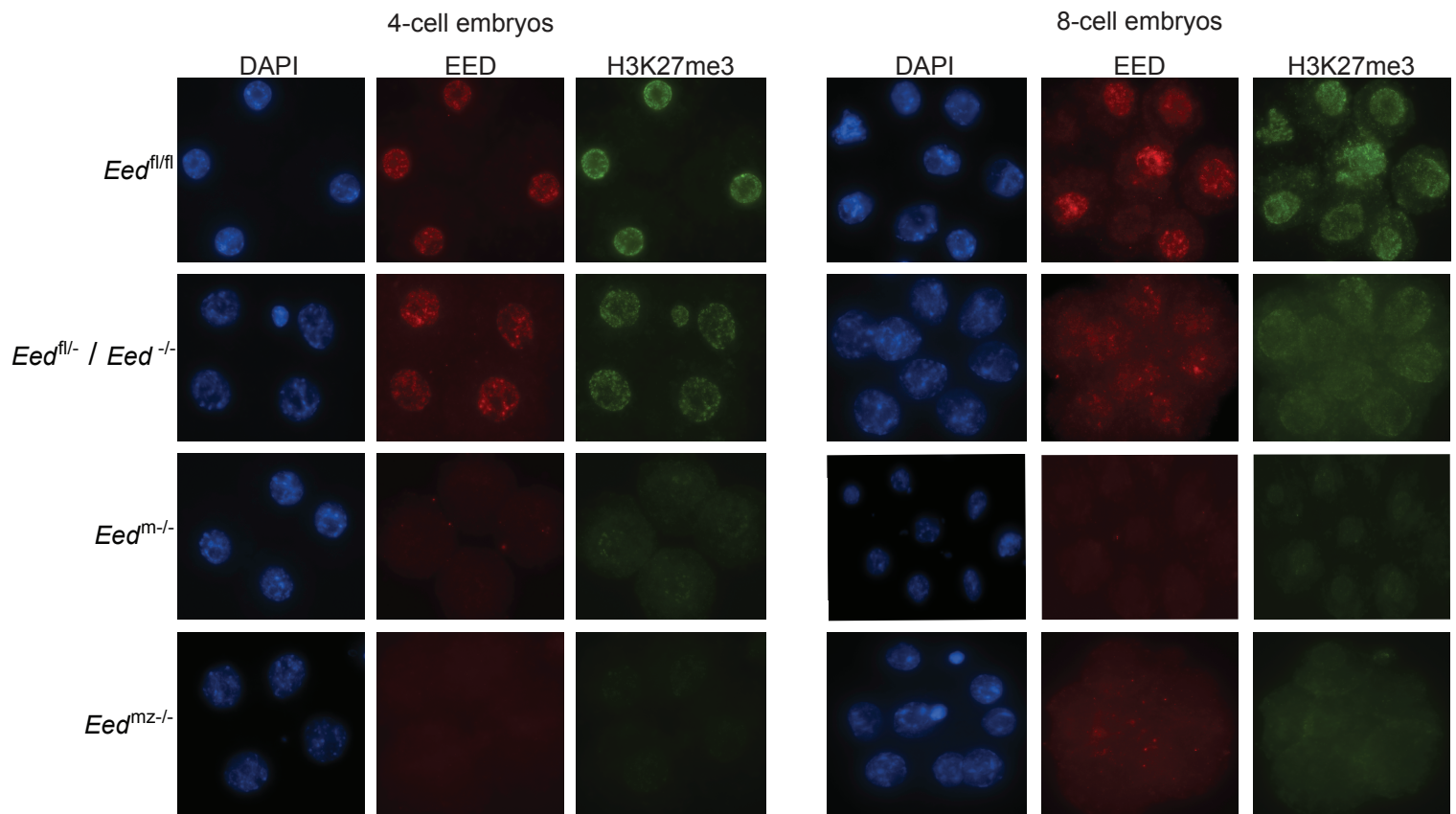
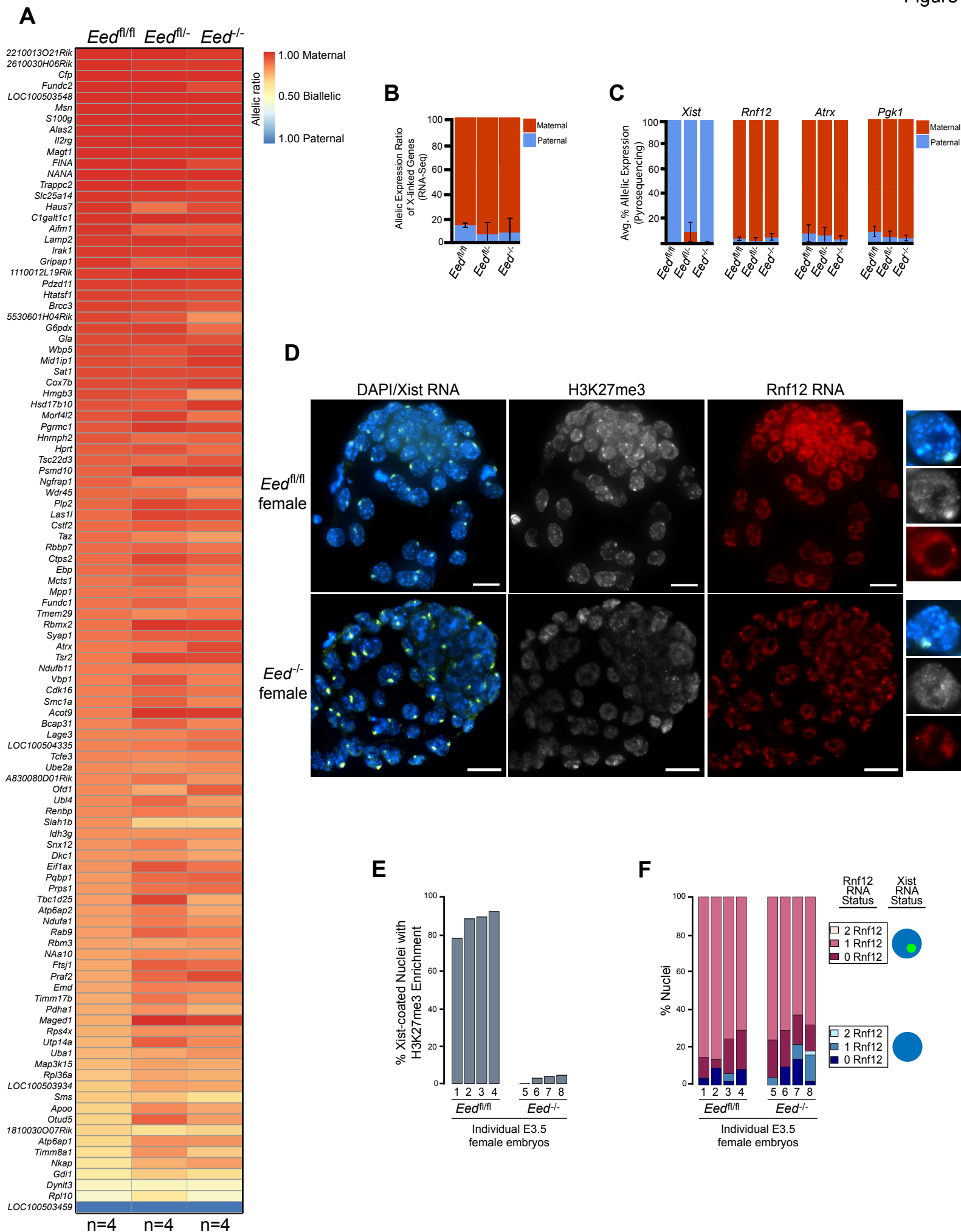
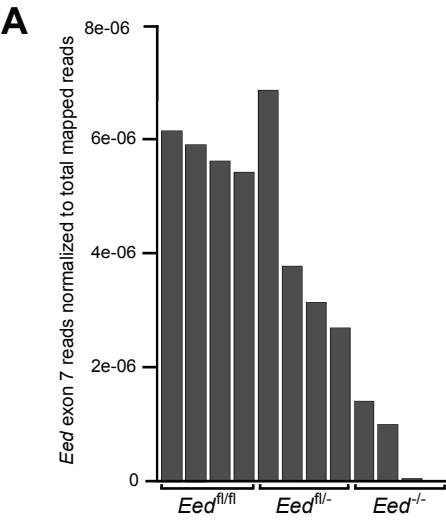
**B**



Figure 3





**B**

Genotype	n	Avg. % Maternal X-linked Gene Expression	Avg. SNP-overlapping Reads per X-linked Gene	SNP Coverage Threshold
<i>Eed</i> <sup>fl/fl</sup>	4	85	4	10
<i>Eed</i> <sup>fl/+</sup>	4	90	4	10
<i>Eed</i> <sup>-/-</sup>	4	88	4	10

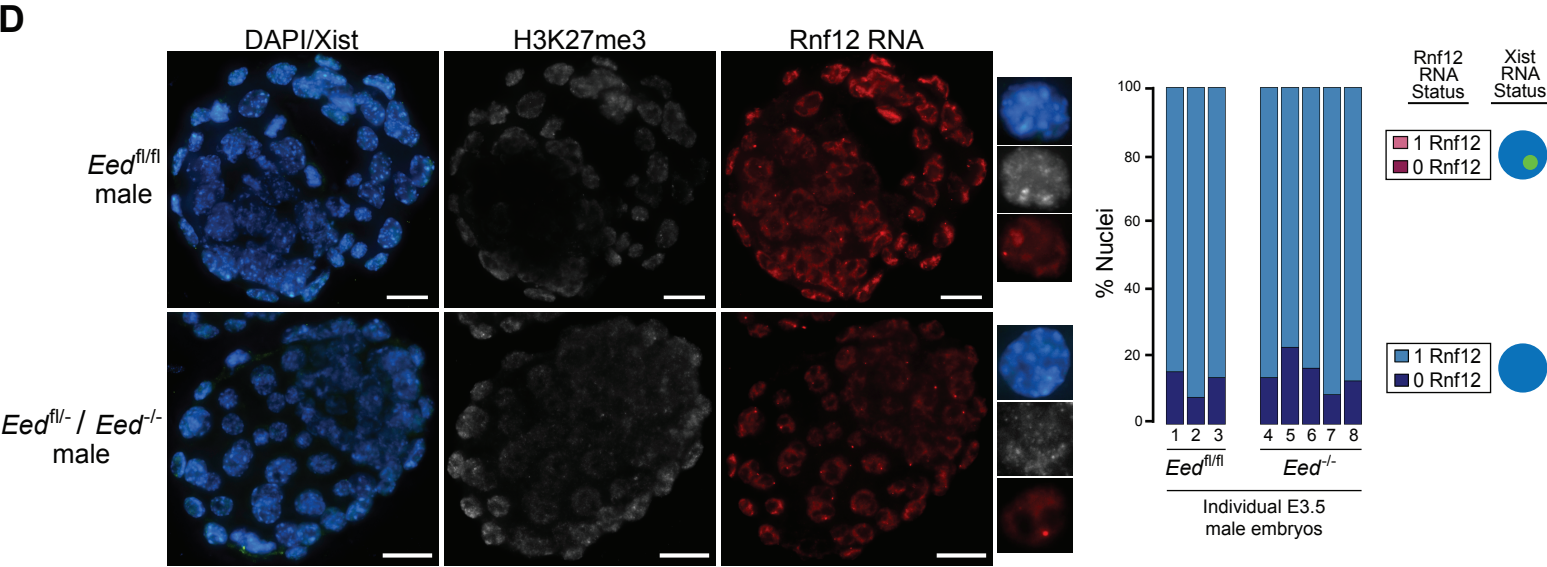
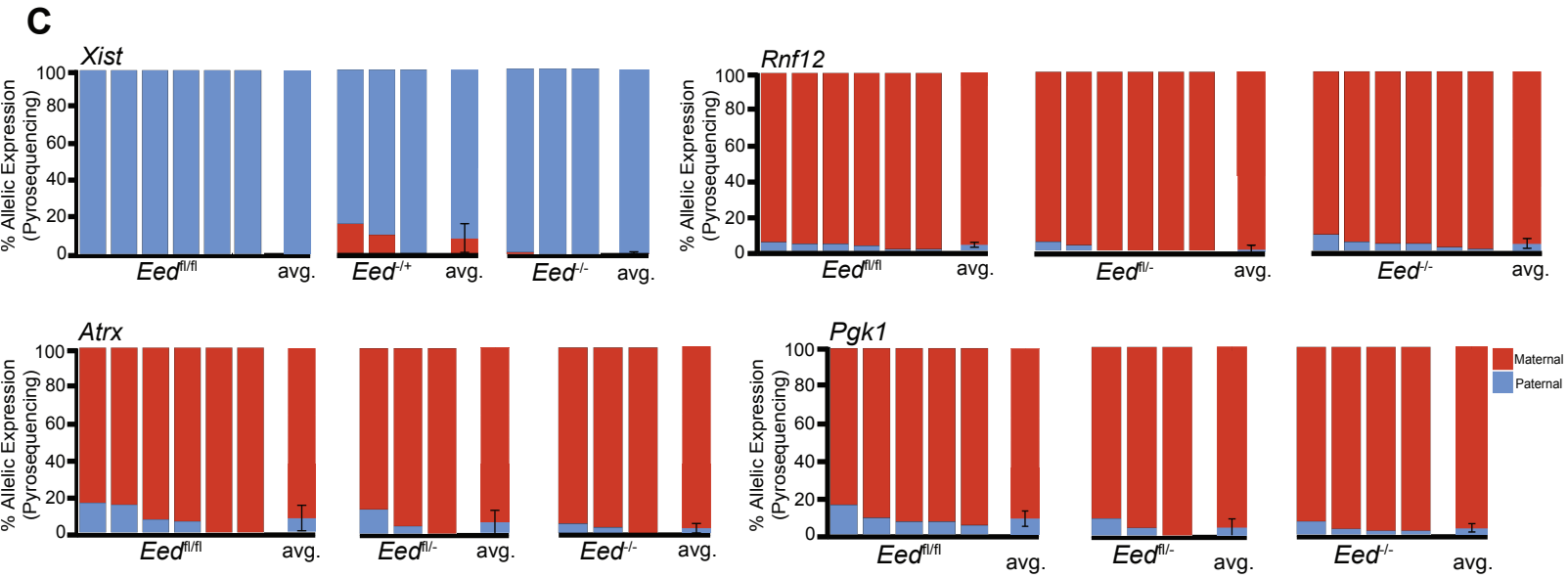
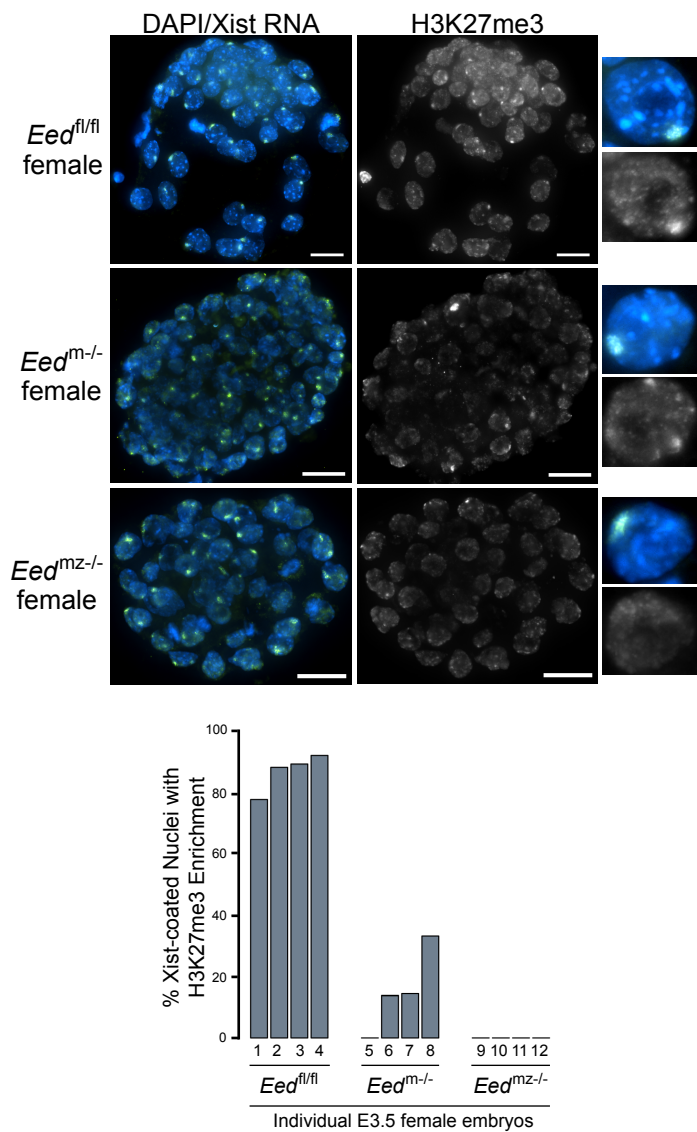
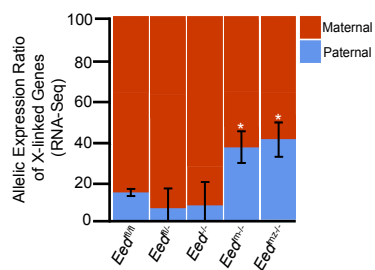
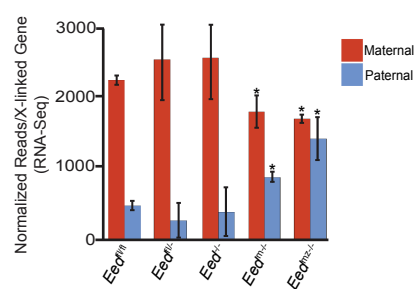
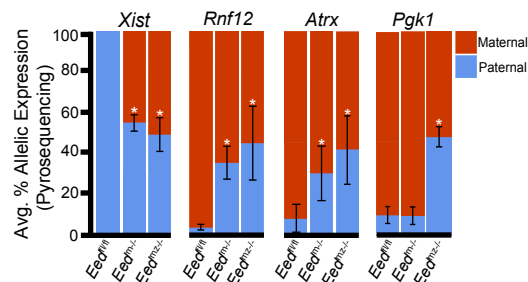
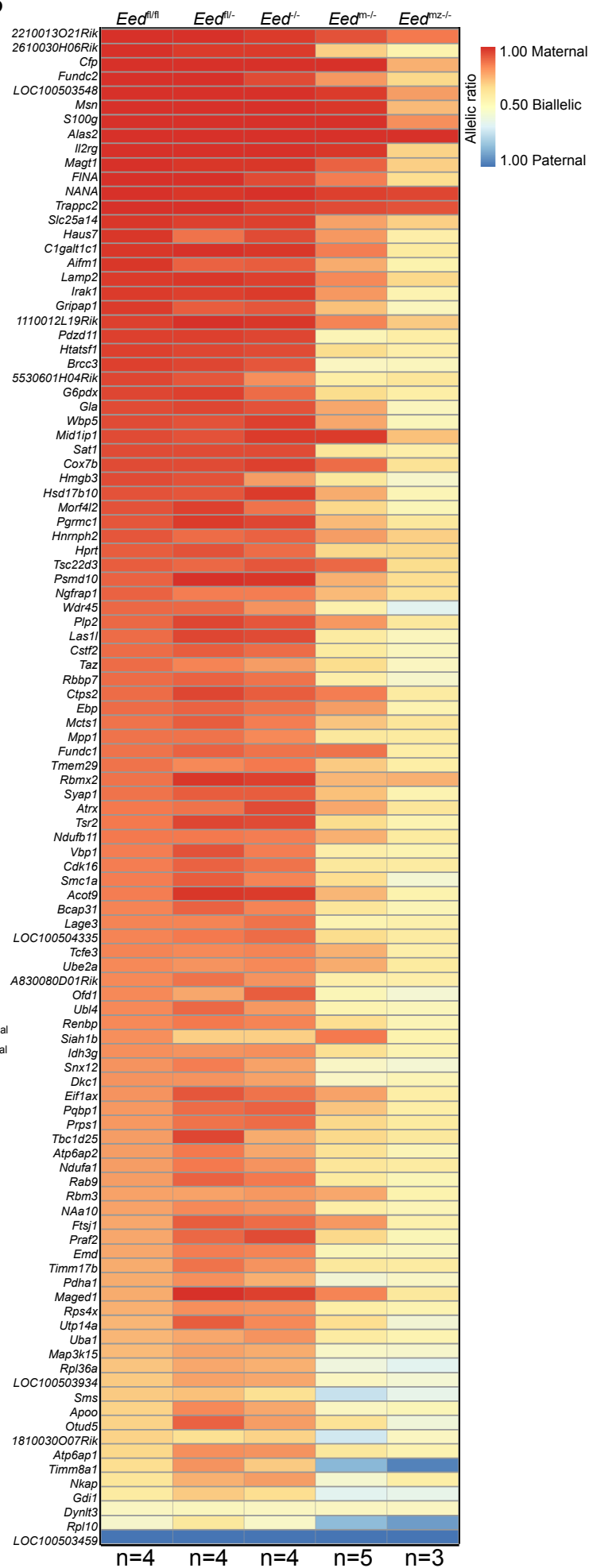
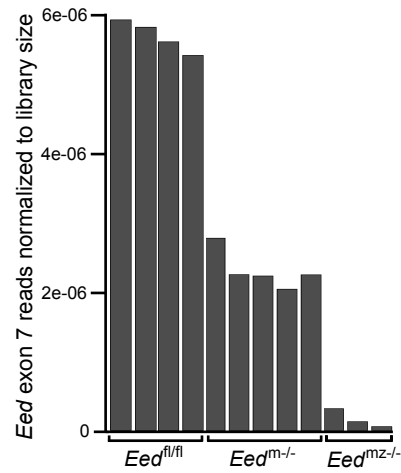


Figure 4

**A****C****D****E****B**

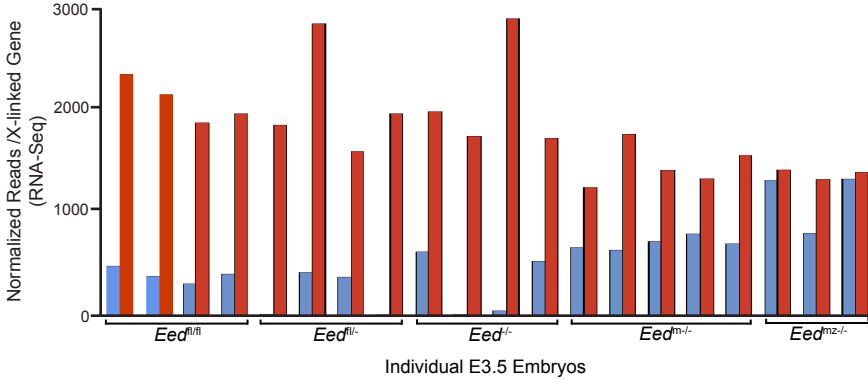
**A**



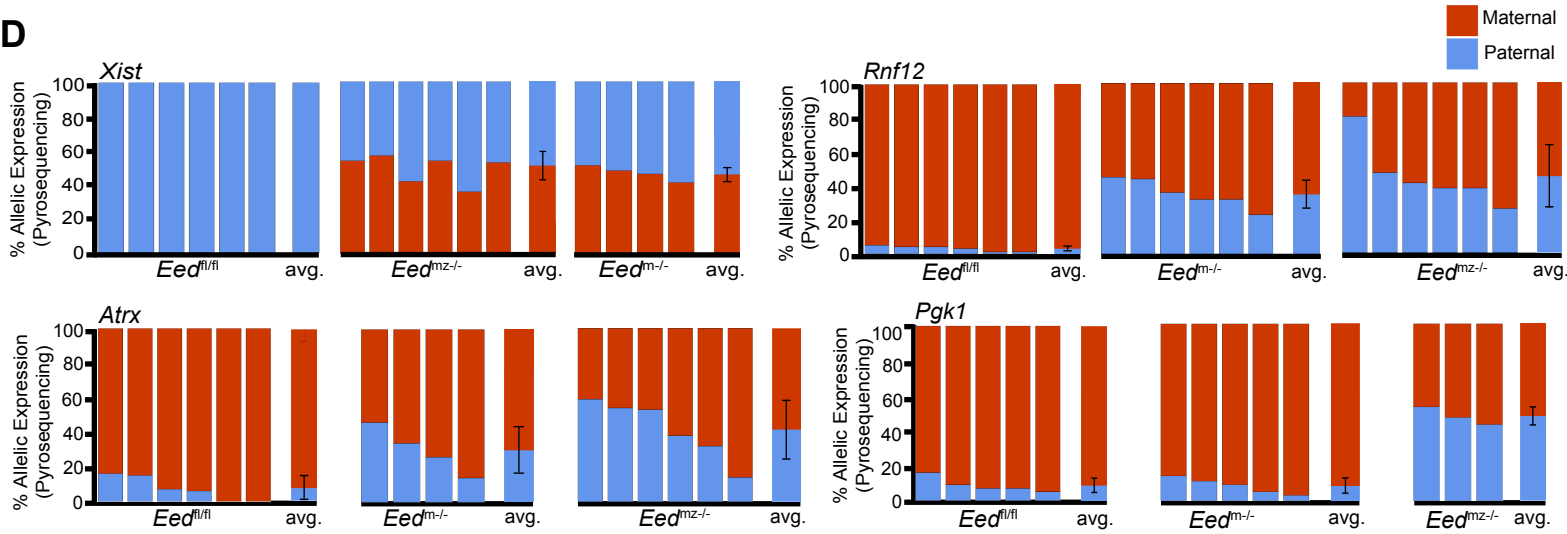
**B**

Genotype	n	Avg. % Maternal X-linked Gene Expression	Avg. SNP-overlapping Reads per X-linked Gene	SNP coverage Threshold
<i>Eed</i> <sup>fl/fl</sup>	4	85	4	10
<i>Eed</i> <sup>m/-</sup>	5	66	4	10
<i>Eed</i> <sup>mz/-</sup>	3	57	4	10

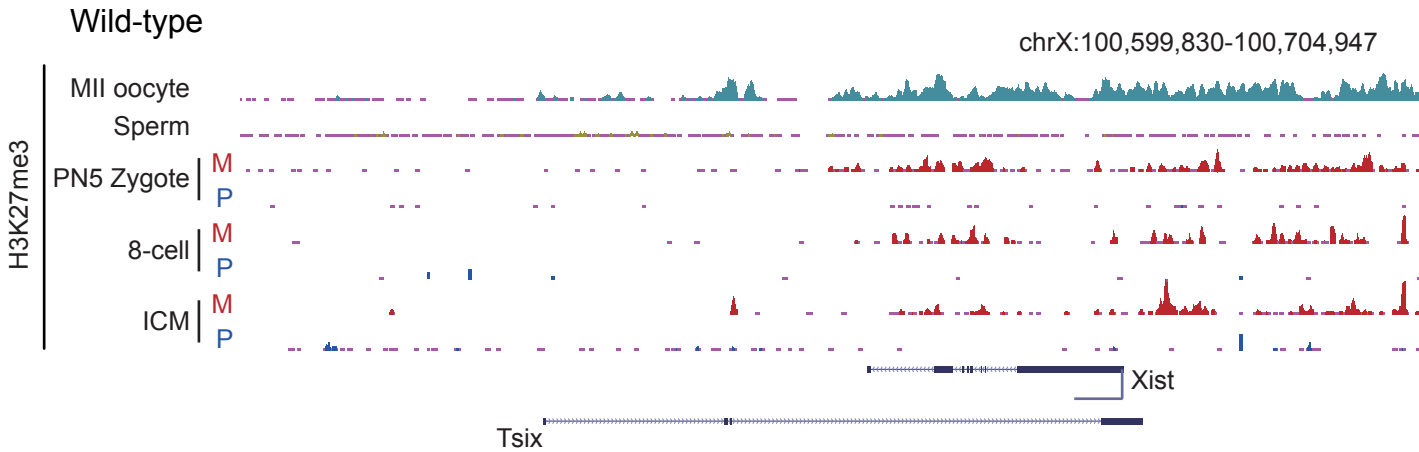
**C**



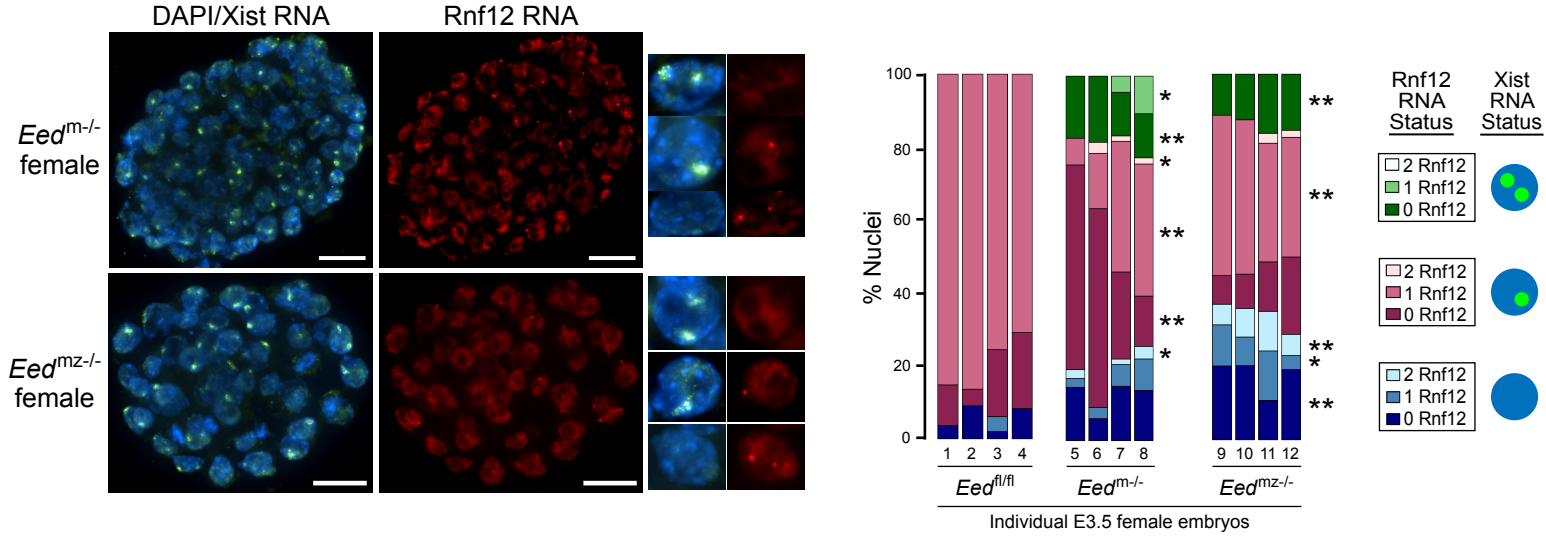
**D**



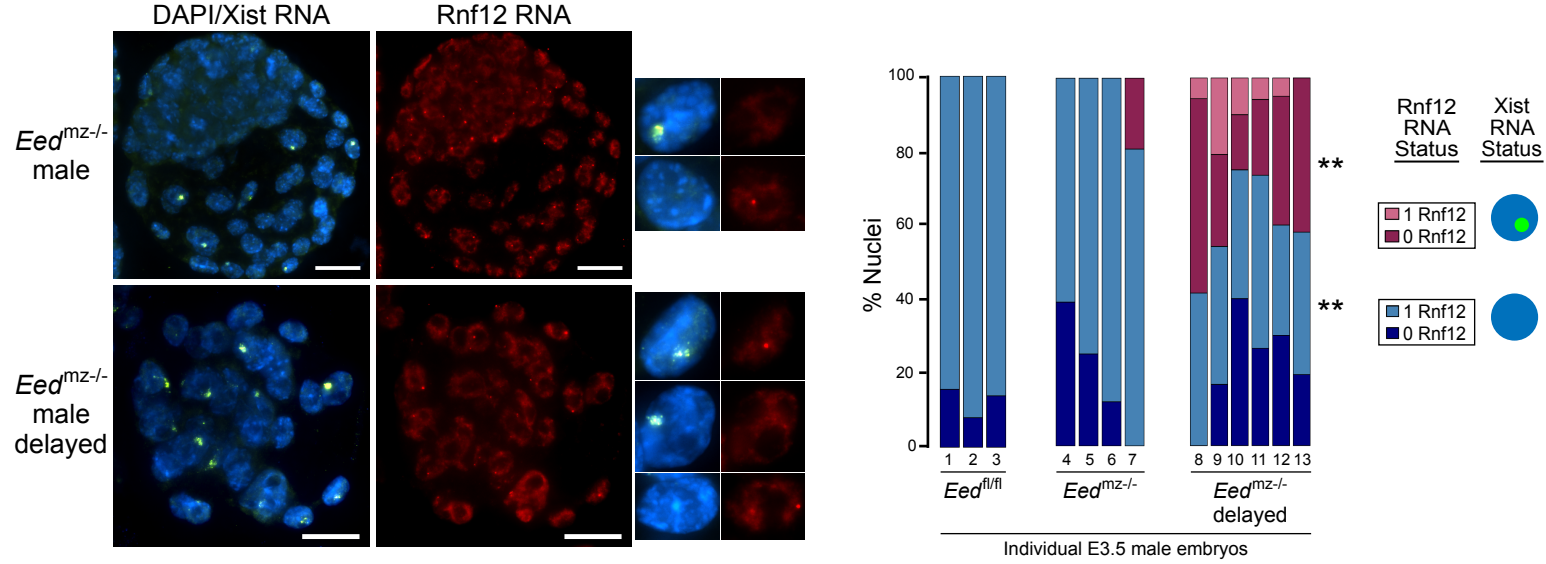
**E**



A



B

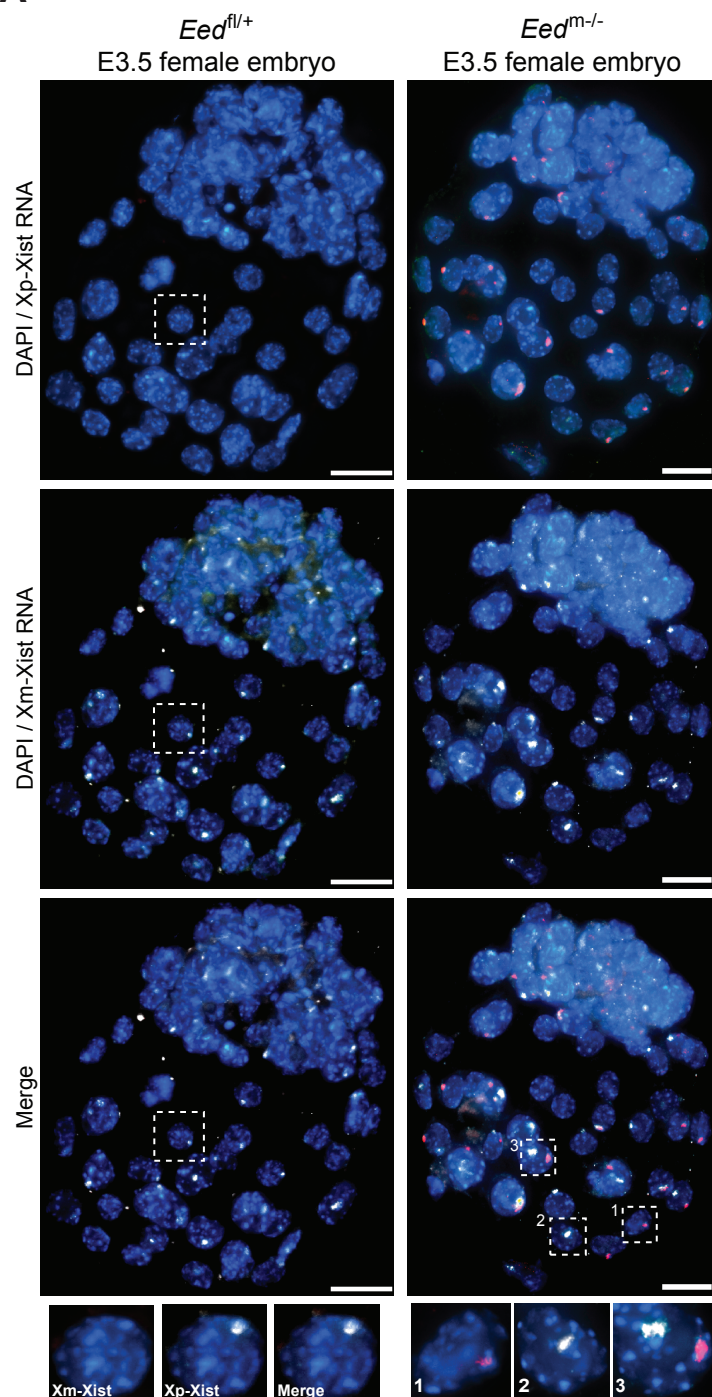
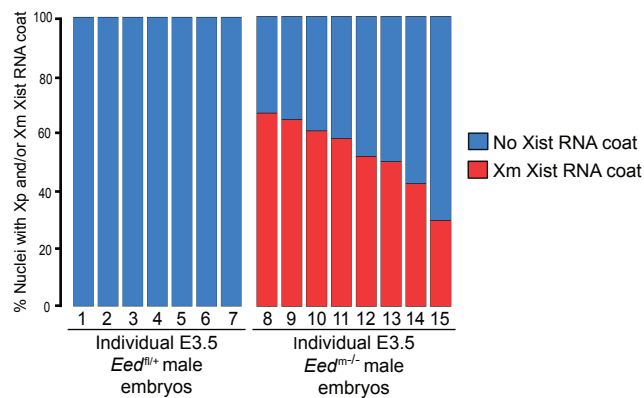
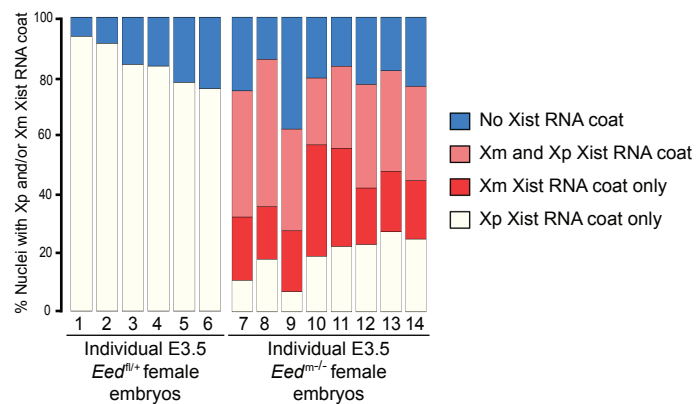
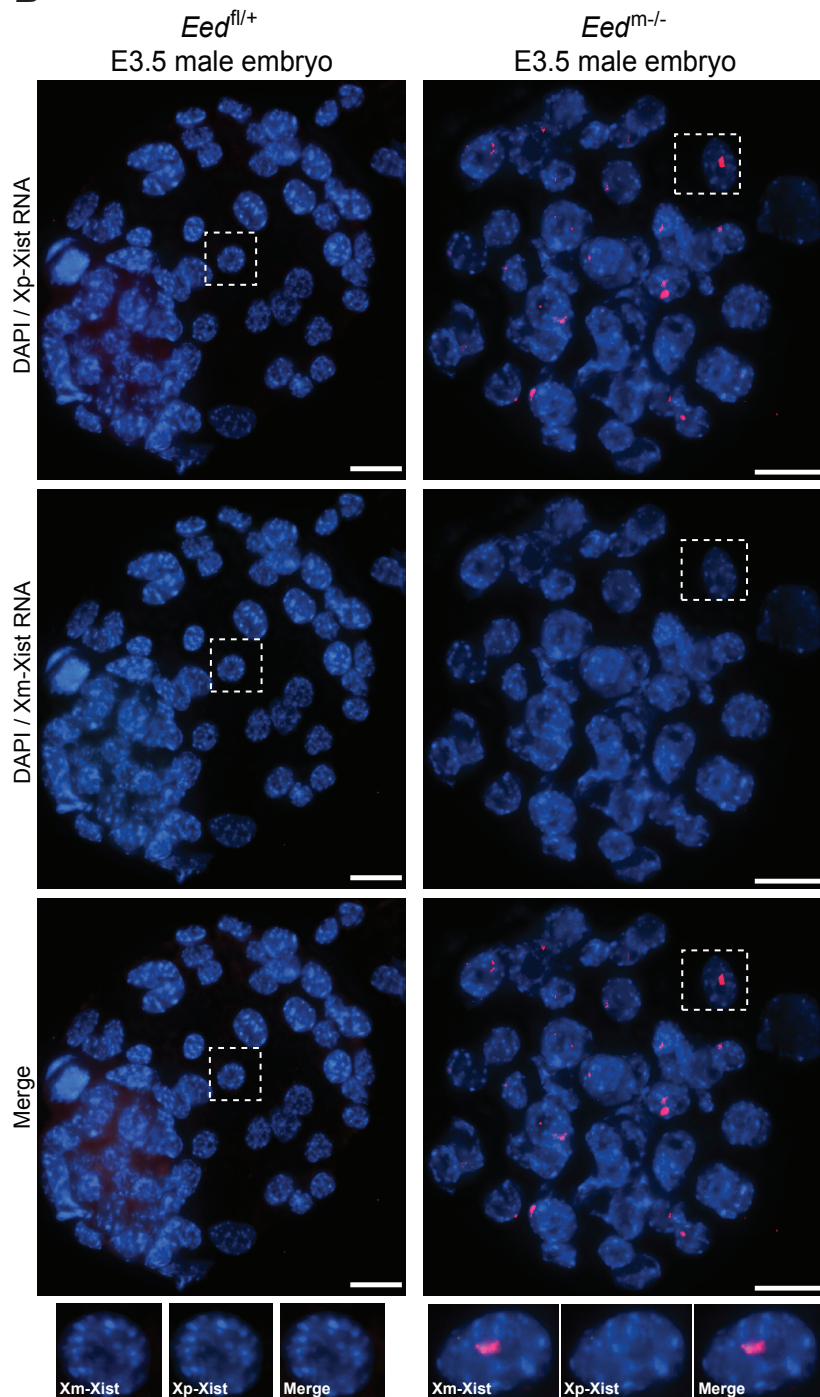


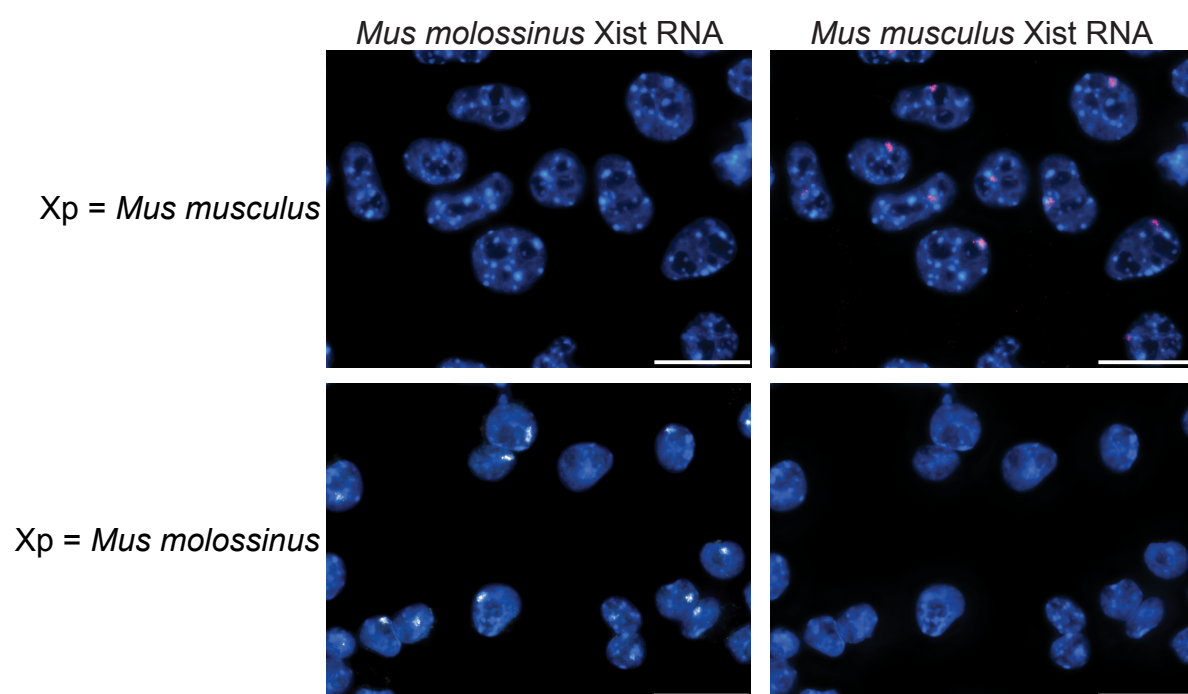
C

*Eed*<sup>m/-</sup> Liveborn Animals

Dam	Sire	Number of litters	Number of pups (avg/litter)	Total females	Total males	<i>Eed</i> <sup>fl/fl</sup> pups	<i>Eed</i> <sup>+/-</sup> pups
<i>Eed</i> <sup>fl/fl</sup>	<i>Mus musculus</i> -derived <i>Eed</i> <sup>fl/fl</sup>	9	61 (6.8)	31 (53%)	30 (47%)	61	0
<i>Eed</i> <sup>fl/fl</sup> ;Zp3-Cre	<i>Mus musculus</i> -derived WT	5	12 (2.4)	9 (75%)	3 (25%)	0	12
<i>Eed</i> <sup>fl/fl</sup> ;Zp3-Cre	<i>Mus molossinus</i> -derived WT	4	10 (2.5)	7 (70%)	3 (30%)	0	10



**A****B**

**A****B**